Metabolic Engineering 67 (2021) 293–307

Contents lists available at ScienceDirect

Metabolic Engineering

journal homepage: www.elsevier.com/locate/meteng

Cascaded valorization of brown seaweed to produce L-lysine and value-added products using *Corynebacterium glutamicum* streamlined by systems metabolic engineering

Sarah Lisa Hoffmann [a], Michael Kohlstedt [a], Lukas Jungmann [a], Michael Hutter [b], Ignacio Poblete-Castro [c], Judith Becker [a], Christoph Wittmann [a,*]

[a] Institute of Systems Biotechnology, Saarland University, Saarbrücken, Germany
[b] Centre for Bioinformatics, Saarland University, Saarbrücken, Germany
[c] Biosystems Engineering Laboratory, Universidad Andres Bello, Santiago, Chile

ARTICLE INFO

Keywords:
Transhydrogenase
Fructokinase
Glyceraldehyde 3-phosphate dehydrogenase
Mannitol 2-dehydrogenase
Protein engineering
NADH
NADPH
Redox balancing
L-lysine
Oxidative pentose phosphate pathway
Fructose
Seaweed
Macro algae

ABSTRACT

Seaweeds emerge as promising third-generation renewable for sustainable bioproduction. In the present work, we valorized brown seaweed to produce L-lysine, the world's leading feed amino acid, using *Corynebacterium glutamicum*, which was streamlined by systems metabolic engineering. The mutant *C. glutamicum* SEA-1 served as a starting point for development because it produced small amounts of L-lysine from mannitol, a major seaweed sugar, because of the deletion of its arabitol repressor AtlR and its engineered L-lysine pathway. Starting from SEA-1, we systematically optimized the microbe to redirect excess NADH, formed on the sugar alcohol, towards NADPH, required for L-lysine synthesis. The mannitol dehydrogenase variant MtlD D75A, inspired by 3D protein homology modelling, partly generated NADPH during the oxidation of mannitol to fructose, leading to a 70% increased L-lysine yield in strain SEA-2C. Several rounds of strain engineering further increased NADPH supply and L-lysine production. The best strain, SEA-7, overexpressed the membrane-bound transhydrogenase *pntAB* together with codon-optimized *gapN*, encoding NADPH-dependent glyceraldehyde 3-phosphate dehydrogenase, and *mak*, encoding fructokinase. In a fed-batch process, SEA-7 produced 76 g L^{-1} L-lysine from mannitol at a yield of 0.26 mol mol^{-1} and a maximum productivity of 2.1 g L^{-1} h^{-1}. Finally, SEA-7 was integrated into seaweed valorization cascades. Aqua-cultured *Laminaria digitata*, a major seaweed for commercial alginate, was extracted and hydrolyzed enzymatically, followed by recovery and clean-up of pure alginate gum. The residual sugar-based mixture was converted to L-lysine at a yield of 0.27 C-mol C-mol^{-1} using SEA-7. Second, stems of the wild-harvested seaweed *Durvillaea antarctica*, obtained as waste during commercial processing of the blades for human consumption, were extracted using acid treatment. Fermentation of the hydrolysate using SEA-7 provided L-lysine at a yield of 0.40 C-mol C-mol^{-1}. Our findings enable improvement of the efficiency of seaweed biorefineries using tailor-made *C. glutamicum* strains.

1. Introduction

There has been a rapid growth of interest in using sustainable resources for the manufacture of industrial chemicals. One of the most important products among the bio-based sectors is L-lysine. This essential amino acid is the world's leading feed supplement (Wittmann and Becker, 2007) and finds further application in the polymer, cosmetic, and pharmaceutical industries (Koffas and Stephanopoulos, 2005). The global L-lysine market grows by 6–7% annually, and the production volume is expected to reach 4 million tons in 2023 (Cheng et al., 2018; Eggeling and Bott, 2015). Currently, the L-lysine industry is based on fermentation using cane and beet molasses and starch hydrolysates from corn, cassava and wheat (Ikeda, 2003; Wittmann and Becker, 2007). However, these raw materials are derived from food crops and suffer from competition with human nutrition (Alaswad et al., 2015). The increasing need for a more sustainable L-lysine production industry has shifted interest towards non-edible second-generation (2G) renewables rich in lignocellulose, such as straw, wood and grass (Balat, 2011;

* Corresponding author. Campus A1.5, 66123, Saarbrücken, Germany.
E-mail address: christoph.wittmann@uni-saarland.de (C. Wittmann).

https://doi.org/10.1016/j.ymben.2021.07.010
Received 23 December 2020; Received in revised form 23 June 2021; Accepted 22 July 2021
Available online 24 July 2021

Buschke et al., 2013a; Naik et al., 2010). As an example, engineered strains of the soil bacterium *Corynebacterium glutamicum* produce L-lysine from lignocellulosic sugars (Anusree et al., 2016; Chen et al., 2019; Gopinath et al., 2011). However, lignocellulosic biomass production is challenged by the need for valuable arable land and the harsh pretreatment required to yield fermentable sugar, consuming high amounts of energy and causing toxin formation (Balat, 2011; Buschke et al., 2013b).

In this context, marine macroalgae (seaweed) show exciting potential as third-generation (3G) feedstock to derive L-lysine in the future (Poblete-Castro et al., 2020). Seaweed, farmed in the oceans and collected from wild stocks, does not require fresh water, chemical fertilizer, arable land, and extreme human intervention (Goh and Lee, 2010; Torres et al., 2019). It offers even higher yields per hectare than leading terrestrial crops (Haag, 2007; Kraan, 2013) and requires only mild and simple extraction for the recovery of fermentable carbohydrates (Poblete-Castro et al., 2020). Moreover, the high photosynthetic activity and rapid growth of seaweed (Alaswad et al., 2015; van Hal et al., 2014) counteracts global warming by fixing CO_2 from the environment (Kraan, 2013). Pioneering efforts have demonstrated the fermentative conversion of seaweed sugars, e.g., to biofuels using yeast (Adams et al., 2011; Enquist-Newman et al., 2014; Sunwoo et al., 2019). Currently, more than 30 million tons of seaweed are farmed in the oceans, and the market volume is expected to increase to 500 million tons by 2050 (Poblete-Castro et al., 2020). Macroalgae are rich in carbohydrates such as polysaccharide alginate and the free sugar alcohol mannitol (Poblete-Castro et al., 2020; Torres et al., 2019; Wei et al., 2013). Depending on season and species, carbohydrate levels as high as 55% are observed (Kraan, 2013; Torres et al., 2019; Wei et al., 2013).

Previously, our group optimized *C. glutamicum* for the production of L-lysine (Becker et al., 2011), ectoine (Becker et al., 2013; Gießelmann et al., 2019), 1,5-diaminopentane (Kind et al., 2014), 5-aminovalerate (Rohles et al., 2016), and glutarate (Rohles et al., 2016, 2018), all of which were produced from glucose.

Here, we describe systems metabolic engineering of *C. glutamicum* for high-level L-lysine production from mannitol and mannitol-based seaweed hydrolysates. *C. glutamicum* seemed a straightforward host to enable L-lysine production from seaweed because it has been the leading workhorse for industrial L-lysine manufacture (Becker and Wittmann, 2012). Recently, the microbe could be modified to produce L-lysine from mannitol, one of the seaweed sugars (Hoffmann et al., 2018), which involved deletion of the arabitol repressor protein AtlR (Laslo et al., 2012), also known as mannitol repressor MtlR and SucR (Peng et al., 2011). In this work, the basic producer *C. glutamicum* SEA-1 served as a starting point for development because it produced at least low amounts of the amino acid from mannitol (Hoffmann et al., 2018). Investigation of intracellular pathway fluxes and pools of reducing equivalents during strain engineering revealed bottlenecks that were caused by unfavourable thermodynamics and a perturbed redox metabolism that limited production efficiency. The advanced producer *C. glutamicum* SEA-7, obtained after several rounds of optimization, was evaluated in a fed-batch process. Subsequently, SEA-7 was successfully used to valorise two commercially relevant seaweeds, namely, *Laminaria digitata* and *Durvillaea antarctica*.

2. Materials and methods

2.1. Microorganisms and plasmids

The basic L-lysine-producing strain *C. glutamicum* SEA-1 was used as starting point for strain engineering (Hoffmann et al., 2018). The *E. coli* strains DH5α and NM522 were obtained from Invitrogen (Karlsruhe, Germany) and used as hosts for plasmid amplification and methylation, respectively. For genomic modification, the integrative plasmid pClik int *sacB* was applied (Becker et al., 2005). This vector contained a multiple cloning site, an origin of replication (ORI) for *E. coli*, kanamycin resistance (kan^R) and the *sacB* gene from *Bacillus subtilis*, encoding levansucrase, used as a selection marker (Jäger et al., 1992, 1995). The plasmid pClik 5α MCS was used for plasmid-based overexpression in *C. glutamicum* (Buschke et al., 2011). It contained a multiple coning site, an ORI for *E. coli* and *C. glutamicum*, an open reading frame encoding the Rep protein to initiate replication of the vector, and kan^R as a selection marker. The plasmid pTC, encoding the DNA methyltransferase for *C. glutamicum*, was used for DNA methylation (Kind et al., 2010). The vector also contained an ORI for *E. coli* and tetracycline resistance (tet^R). To add the DNA methylation pattern of *C. glutamicum* to plasmid DNA, pTC was co-expressed in *E. coli* NM522. All strains and plasmids used in this study are displayed in Table 1.

2.2. Molecular design and genetic engineering

For cloning design, the software Clone Manager Professional 9 (Sci-Ed Software, Denver, CO, USA) was applied. The amplification of DNA fragments, the construction of transformation vectors, and their transformation into *E. coli* via heat shock were performed as described

Table 1
Corynebacterium glutamicum strains and plasmids.

Strain/ Plasmid	Description	Reference
Strain		
SEA-1	LYS-12 + deletion of *atlR* (*mtlR*) (NCgl0110)	(Hoffmann et al., 2018)
SEA-2C	SEA-1 + nucleotide exchange in the *mtlD* gene (NCgl0108) of *C. glutamicum*, encoding mannitol 2-dehydrogenase, resulting in the mutation D75A	This work
SEA-2D	SEA-1 + genome-based integration of *pntAB* (EG10744, EG10745) from *E. coli* K12-MG1655, encoding the membrane-bound nicotinamide nucleotide transhydrogenase PntAB, into the *crtB* gene locus (NCgl0598)	This work
SEA-4	SEA-2B + genome-based integration of *pntAB* (EG10744, EG10745) from *E. coli* K12-MG1655, encoding the membrane-bound nicotinamide nucleotide transhydrogenase PntAB, into the *crtB* gene locus (NCgl0598)	This work
SEA-5	SEA-4 + empty plasmid pClik 5a MCS	This work
SEA-6	SEA-4 + plasmid-based expression of *gapN* (SMU_676) from *S. mutans* UA159, encoding NADP-dependent glyceraldehyde 3-phosphate dehydrogenase	This work
SEA-7	SEA-4 + genome-based integration of codon-optimized *gapN* (SMU_676) from *S. mutans* UA159, encoding NADP-dependent glyceraldehyde 3-phosphate dehydrogenase, into the *crtI*2 gene locus (NCgl0597)	This work
Plasmid		
pTC	Expression vector for DNA methyltransferase of *C. glutamicum*, containing an origin of replication (ORI) for *E. coli* and tet^R as a selection marker	(Kind et al., 2010)
pClik int *sacB*	Integrative transformation vector for genome-based modification, comprising an MCS for *C. glutamicum*, an ORI for *E. coli*, and kan^R and *sacB* as selection markers	Becker et al. (2005)
pClik 5a MCS	Episomal vector	Buschke et al. (2011)
pClik 5a MCS *gapN*	Episomal vector with native *gapN* from *S. mutans* UA159 (SMU_676)	Hoffmann et al. (2018)
pClik int *sacB mtlD**	Integrative transformation vector to replace the GAT start codon of *mtlD* by GCA	This work
pClik int *sacB* P_{tuf} *pntAB*	Transformation vector for integration of the *pntAB* gene from *E. coli* K12-MG1655 into the *crtB* gene locus under control of the *tuf* promoter	This work
pClik int *sacB* P_{tuf} *gapN*	Transformation vector for integration of the codon-optimized *gapN* gene from *S. mutans* UA159 into the *crtI*2 gene locus under control of the *tuf* promoter	This work

previously (Becker et al., 2010; Hoffmann et al., 2018). The final vectors were transformed into *C. glutamicum* by electroporation (Becker et al., 2010). The correctness of each genetic modification was verified by PCR and sequence analysis (GATC Biotech AG, Konstanz, Germany). Further details on the cloning can be found in the **supplementary file 1**, whereby the primer sequences used in this study are listed in Table S1.

2.3. Computational modelling for protein engineering

The crystallographic structure of mannitol 2-dehydrogenase from *Pseudomonas fluorescens* (pdb entry 1M2W.pdb) was retrieved from the RCSB Protein Data Bank (PDB) and used to generate a homology model of the *C. glutamicum* enzyme using SWISS-MODEL (Benkert et al., 2011; Waterhouse et al., 2018). The new cofactor $NADP^+$ was re-constructed on basis of NAD^+, which was present in the X-Ray structure, by adding the corresponding phosphate group manually (the phosphate residue was added to NAD^+ to mimic $NADP^+$), followed by energetic optimization using the MM + force field parameters implemented in HYPERCHEM (HYPERCHEM, 1999) to predict its putative position in the binding site. The native and modified enzyme structures were visualized using Swiss-Pdb Viewer for subsequent inspection of interactions between $NADP^+$ and the protein residues that could be optimized by mutations (Guex et al., 1999).

2.4. Batch cultivation in shake flasks

Cultivation studies in minimal medium were conducted as previously described (Hoffmann et al., 2018). For ^{13}C metabolic flux analysis, naturally labelled mannitol was replaced by 99% [1–^{13}C] mannitol (Omicron Biochemicals, South Bend, IN, USA) (Hoffmann et al., 2018). For cultivation of *C. glutamicum* on seaweed extracts, a chemically defined mineral salt medium without carbon source was prepared as described above. Instead of pure substrate, algal extract was then added to the main culture. The resulting concentration of total sugar is given below.

2.5. Fed-batch cultivation in stirred tank bioreactors

The production performance of *C. glutamicum* on mannitol was assessed in a fed-batch process using 1 L bioreactors (SR0700ODLS, DASGIP AG, Jülich, Germany). The preculture was grown for 12 h at 30 °C in 2 L baffled flasks, filled with 200 mL of complex medium (37 g L^{-1} BHI, 15 g L^{-1} mannitol). Cells were harvested (5 min, 8800×*g*, room temperature), resuspended in 50 mL of batch medium and then used as inoculum. The batch medium contained 41 g of mannitol, 6.6 g of yeast extract (Sigma-Aldrich, Steinheim, Germany), 2 g of citric acid, 25 g of $(NH_4)_2SO_4$, 1.25 g of KH_2PO_4, 1.6 g of $Na_2HPO_4 \cdot 2H_2O$, 1.25 g of $MgSO_4 \cdot 7H_2O$, 70 mg of $FeSO_4 \cdot 7H_2O$, 30 mg of $ZnSO_4 \cdot 7H_2O$, 9 mg of $MnSO_4 \cdot H_2O$, 133 mg of $CaSO_4 \cdot H_2O$, 0.43 mg of boric acid, 0.59 mg of $CoSO_4 \cdot 7H_2O$, 0.63 mg of $CuSO_4 \cdot 5H_2O$, 0.47 mg of $NiSO_4 \cdot 6H_2O$, 0.06 mg of $(NH_4)_2MoO_4$, 4.5 mg of biotin, 9.5 mg of thiamine·HCl, 9 mg of nicotinamide, 33 mg of pantothenic acid, and 1 mL of antifoam 204 (Sigma-Aldrich). The process was started with 300 mL (initial volume) of medium. During the process, the temperature was kept at 30 °C ± 0.1 (CWD4 bioblock, DASGIP AG, Jülich, Germany). For pH monitoring, a pH electrode was used (Mettler Toledo 405-DPAS-SC-K8S/225, Mettler Toledo, Giessen, Germany). A 25% NH_4OH solution was added automatically (MP8 pump system, Eppendorf, Hamburg, Germany) to keep the pH stable at 7.0 ± 0.1. The dissolved oxygen level (pO_2) was monitored using a pO_2 electrode (VisiFerm DO 225; Hamilton, Höchst, Germany), and it was maintained above 30% saturation by adjusting the stirrer speed, aeration rate, and oxygen fraction of the gas inflow. The composition of the exhaust gas (CO_2 and O_2) was measured online (GA4, DASGIP AG, Jülich, Germany). The initial stirrer speed was set to 600 rpm, and the aeration rate was set to 18 sL h^{-1}. The feed solution contained 192 g of mannitol, 14 g of urea, 13.3 g of $(NH_4)_2SO_4$, 5 g of yeast extract (Sigma-Aldrich), 150 mg of biotin, 317.8 mg of thiamine·HCl, 300 mg of nicotinamide, 1.1 g of pantothenic acid, and 1 mL of antifoam 204 (Sigma-Aldrich) per litre. Feed pulses were added when the pO_2 increased to more than 45%. Data acquisition and process control were conducted by the DASGIP control software (DASGIP AG, Jülich, Germany).

2.6. Extraction of the brown seaweed Durvillaea antarctica

D. antarctica was collected in wintertime (August 2019) at Los Molles, Valparaiso, Chile (32°14′36″S, 71°31′00″W). The non-edible parts, i. e. the mid-stem parts, were processed. They were washed with seawater to remove sand and transported to the laboratory in plastic bags. The stem was cut into pieces (10 cm in length), dried at 60 °C until constant weight and powdered with a blender for 15 min. For extraction, 10 g of powder was mixed with 200 mL of ethanol (80% v/v) and stirred at 60 °C for 2 h. Subsequently, the ethanol was evaporated by heating to 80 °C for 30 min. The resulting solution was resuspended in 250 mL of sulphuric acid (4% v/v), autoclaved (121 °C, 40 min), cooled down to room temperature, stirred overnight, and then neutralized to pH 7.0 by adding KOH pellets (>85%). The supernatant was collected (10 min, 6000×*g*, 20 °C) and clarified by filtration (Whatman filter paper 6 μM, 55 mm, GE Health Care, Amersham, UK). The obtained hydrolysate was sterilized (121 °C, 15 min).

2.7. Extraction of the brown seaweed Laminaria digitata

Dried leaves (50 g) of *Laminaria digitata* (Makrobiotik, Hohrenk, Germany) were powdered with a blender. The powder was resuspended in 500 mL of deionized water and autoclaved (121 °C, 18 min), yielding a mannitol-rich hydrolysate. As an optional step, enzymatic hydrolysis was conducted after the heating step to increase the sugar level. For this purpose, the extract was amended with a cocktail of enzymes, i.e., Celluclast 1.5 L (10 mg g^{-1}) and Viscozyme L (10 mg g^{-1}) (Sigma-Aldrich, Steinheim, Germany), and incubated at 50 °C and pH 5.5 for 48 h. Subsequently, the hydrolysate was clarified from debris and collected (15 min, 5000×*g*, 4 °C), and alginate was precipitated as described below.

2.8. Purification of alginate from seaweed extracts

The extraction of sodium alginate from seaweed hydrolysate was adapted from previous work (Haug et al., 1974; Latifi et al., 2015). In short, $CaCl_2 \cdot 2H_2O$ (0.1 g g^{-1}) was added. The mixture was stirred (15 min, 200 rpm). The precipitated raw alginate was separated from the supernatant by filtration, resuspended in 2% (w/v) $CaCl_2$ for 2 h and then washed with deionized water. Subsequently, the polymer was treated for 2 h with 40% formaldehyde and then extracted twice with 50 mL of 0.2 M HCl. Then, it was washed three times with deionized water. Finally, the alginate was dissolved in 400 mL of 3% (w/v) Na_2CO_3 and incubated for two days. Then, the solution was centrifuged (30 min, 10, 000×*g*) to remove solids, and the obtained supernatant was mixed with an equal volume of ethanol to precipitate alginate as sodium salt. Finally, the obtained sodium alginate was washed twice with acetone and dried for 24 h at room temperature and then for 24 h at 80 °C.

2.9. Processing of seaweed hydrolysate for fermentative L-lysine production

The *D. antarctica* extract (see above) was directly used for cultivation experiments, while the *L. digitata* extract was concentrated after alginate separation to achieve a higher carbohydrate content. For this purpose, the alginate-free extract was filtered (Whatman filter paper, 6 μM, 55 mm, GE Health Care, Amersham, UK) and concentrated approximately seven-fold (3 h, Vacuum Concentrator RVC 2-33 IR, Christ, Osterode, Germany), followed by pH adjustment to pH 7.4 with 6 M NaOH. The

final solution was sterilized by autoclaving (121 °C, 20 min) prior to cultivation.

2.10. Substrate and product quantification in culture broth

Quantification of trehalose and organic acids (lactate, acetate) was conducted by isocratic HPLC (1260 Infinity Series, Agilent Technology) using an Aminex HPX-87H column (300 × 7.8 mm, Bio-Rad, Hercules, CA, USA) at 55 °C with 50 mM H_2SO_4 as the mobile phase and a flow rate of 0.5 mL min^{-1} (Hoffmann et al., 2018). Detection and quantification of the analytes were performed via refraction index measurement and with external standards. Mannitol, glucose, and fructose were quantified using HPLC (1260 Infinity Series, Agilent Technology) with a Metacarb 87C column (300 × 7.8 mm, Agilent Technology), preceded by a Metacarb 87C guard column (50 × 7.8 mm, Agilent Technology) and a desalting column (Micro-Guard Deashing Cartridge, Bio-Rad). Separation was carried out at 85 °C using demineralized water as the mobile phase at a flow rate of 0.5 mL min^{-1}. Refraction index measurement was used for detection, and external standards were used for quantification. Quantification of amino acids was conducted as described previously (Hoffmann et al., 2018). The cell concentration was determined spectrophotometrically at 660 nm (OD_{660}) (UV-1600PC spectrophotometer, VWR, Hannover, Germany). The concentration of the cell dry mass (CDM) was calculated from the optical density using the formula CDM [g L^{-1}] = 0.352 x OD_{660}, wherein the correlation factor was previously determined for mannitol-grown *C. glutamicum* (Hoffmann et al., 2018).

2.11. Quantification of intracellular carbohydrates

To quantify fructose and mannitol in cell extracts, 5 mg biomass was harvested by vacuum filtration using cellulose nitrate filters (0.2 μm pore size, 47 mm, Sartorius, Göttingen, Germany) and washed twice with 2.5% NaCl. The filter was then placed into a cup, pre-filled with 2 mL D-galactose solution (250 μM) as internal standard. The cup was then closed and incubated for 15 min at 100 °C for metabolite extraction. Then, the solution was cooled on ice (10 min) and clarified from debris (13,000×*g*, 5 min, 4 °C). For quantification of intracellular carbohydrates, the obtained extract was dried (4 h, Vacuum Concentrator RVC 2-33 IR, Christ, Osterode, Germany), followed by a two-step conversion of the sugars into the corresponding trimethylsilyl *O*-methyloxime derivates. For this purpose, the extract was dissolved in 50 μL pyridine (2% methoxylamine) and incubated for 25 min at 80 °C. Afterwards, 50 μL *N, O-bis*-trimethylsilyl-trifluoroacetamide (BSTFA, Macherey-Nagel, Düren, Germany) was added and the mixture was incubated for 30 min at 80 °C (Kiefer et al., 2004; Schwechheimer et al., 2018). Subsequently, the derivatized extract was analysed by gas chromatography-mass spectrometry (GC-MS) (GC 7890A, 5975C quadrupole detector, Agilent Technologies) (Kiefer et al., 2004; Krömer et al., 2008; Wittmann et al., 2002), using the following temperature gradient: 0–3 min 150 °C, 3–10 min linear increase to 230 °C, 10–14 min linear increase to 325 °C.

To exclude isobaric interference between the analytes of interest and the sample matrix, all samples were first measured in scan mode (Wittmann, 2007). The mass isotopomer distributions (MIDs) of fructose, mannitol, and the internal standard galactose were then determined in duplicate via selective ion monitoring (SIM) of the most prominent ion clusters. These were inferred from the analysis of pure standards and the MassBank Europe mass spectral database (www.massbank.eu): fructose, *m/z* 103-105, 147-149, 217-219, and 307-309 (MassBank record RP023511); mannitol *m/z* 103-105, 205-207, 307-309, 319-321 (MassBank record OUF00344); galactose *m/z* 73-75, 103-105, 147-149, and 319-321 (MassBank record PR010044). Initial tests aimed to use LC-ESI-MS/MS for the quantification of intracellular fructose and mannitol. Trials on a triple quadrupole MS (QTRAP 6500+, AB Sciex, Darmstadt, Germany) coupled to an HPLC system (Agilent Infinity 1290 System) with a reversed phase column (Gemini C18, 100 mm × 4.6 mm, 3 μm, 110 Å, Phenomenex, Aschaffenburg, Germany) (Gläser et al., 2020), however, revealed insufficient separation of the analytes of interest in cell extracts so that this approach was not considered further.

2.12. Identification of sugars in seaweed hydrolysates

To identify the carbohydrates contained in seaweed hydrolysate, 1 mL extract was dried at 80 °C for approximately 20 h. Subsequently, 400 μL of HCl (2 M) was added. Then, the solution was clarified by filtration (0.2 μm, Merck, Millipore, Darmstadt, Germany) and dried under nitrogen for approximately 20 min. Further sample preparation included a two-step derivatization as previously described (Kiefer et al., 2004; Schwechheimer et al., 2018), however, another silylation reagent was used. In short, the dried supernatant was incubated in 50 μL of pyridine (2% methoxylamine) for 25 min at 80 °C and then derivatized with 50 μL of *N*-methyl-*N*-trimethylsilyl-trifluoroacetamide (MSTFA, Macherey-Nagel, Düren, Germany) for 30 min at 80 °C. The subsequent analysis in scan mode was carried out by gas chromatography-mass spectrometry (GC-MS) (GC 7890A, 5975C quadrupole detector, Agilent Technologies) using pure standards as a reference (Kiefer et al., 2004; Krömer et al., 2008; Wittmann et al., 2002).

2.13. GC-MS ^{13}C analysis of proteinogenic amino acids

For ^{13}C labelling analysis, mass isotopomer distributions (MIDs) of amino acids from the cell protein of *C. glutamicum* were quantified by GC-MS (GC 7890A, 5975C quadrupole detector, Agilent Technologies) as described previously (Hoffmann et al., 2018). The obtained MIDs were corrected for natural isotope abundance (van Winden et al., 2002).

2.14. Metabolic modelling and flux estimation

Metabolic flux analysis of mannitol-grown *C. glutamicum* was conducted as described previously (Hoffmann et al., 2018). To additionally capture fluxes through the introduced transhydrogenase and malic enzyme, the approach was extended, considering the *in vitro* activities of the enzymes as constraints and consistency checks (Lange et al., 2017). The cultures exhibited isotopic and metabolic steady state (Fig. S1; Fig. S2, supplementary file 1). Using ^{13}C labelling information of proteinogenic L-alanine (Table S2, supplementary file 1), measured extracellular fluxes (Table S3, supplementary file 1), and metabolite balancing, the approach provided a distribution of intracellular carbon fluxes through the metabolism of *C. glutamicum* **(Tables S4 - S13, supplementary file 1).**

2.15. Determination of enzyme activities

To prepare crude cell extract, cells were grown, harvested, and disrupted as described previously (Hoffmann et al., 2018). All assays were conducted in triplicate. For the analysis of mannitol 2-dehydrogenase activity, crude cell extract was obtained using 100 mM Tris-HCl (pH 7.8, 10 mM $MgCl_2$, 0.75 mM DTT) as disruption buffer. Activity measurement was performed in 1 mL of buffer containing 25 μL of crude cell extract, 80 mM mannitol, and 1 mM NAD^+ at 30 °C (Peng et al., 2011). For kinetic studies, the concentration of NAD^+ was varied, and the cofactor was replaced by $NADP^+$. An extinction coefficient of ϵ_{340} = 6.22 L $mmol^{-1}$ cm^{-1} for NAD(P)H was used to determine the enzyme activity based on the change in absorbance at 340 nm.

For determination of glyceraldehyde 3-phosphate dehydrogenase activity, cells were disrupted in 100 mM Tris-HCl (pH 8.3, 10 mM $MgCl_2$, 0.75 mM DTT). The activity of the enzyme was measured at 30 °C in 1 mL of 100 mM Tris-HCl buffer containing 25 μL of crude extract, 2 mM glyceraldehyde 3-phosphate, and either 1 mM NAD^+ or 1 mM $NADP^+$ to assay both variants, i.e., native NAD-dependent glyceraldehyde 3-phosphate dehydrogenase (GapA) and NADP-dependent glyceraldehyde 3-

phosphate dehydrogenase (GapN). An extinction coefficient of ϵ_{340} = 6.22 L $mmol^{-1}$ cm^{-1} for NAD(P)H was used to determine the enzyme activity based on the change in absorbance at 340 nm.

To measure malic enzyme activity, cells were disrupted in a buffer containing 100 mM Tris-HCl (pH 7.8, 200 mM KCl, 0.75 mM DTT). The enzyme activity was then analysed at 30 °C as described previously (Gourdon et al., 2000) using a total volume of 1 mL, containing 100 mM Tris-HCl (pH 7.8), 200 mM KCl, 2 mM $MgCl_2$, 1 mM NADP, 40 mM malate, and 50 μL of crude extract. An extinction coefficient of ϵ_{340} = 6.22 L $mmol^{-1}$ cm^{-1} for NAD(P)H was used to determine the enzyme activity based on the change in absorbance at 340 nm.

Prior to activity analysis, membrane-bound transhydrogenase (PntAB) was enriched as the membrane fraction from cells, harvested by centrifugation (10 min, 4500×*g*, 4 °C), and washed with TE buffer (10 mM Tris-HCl, 1 mM EDTA; pH 8.0) as described previously (Kabus et al., 2007). The cell pellet was resuspended in 1 mL of TE buffer containing 40 μL of complete protease inhibitor (Roche Diagnostics, Penzberg, Germany). Cells were then transferred into FastPrep-24 vials and disrupted as described above. Cell debris was removed by centrifugation (20 min, 5000×*g*, 4 °C). The obtained crude extract was subjected to ultracentrifugation (90 min, 150,000×*g*, 4 °C). The sedimented membrane fraction was washed in 1 mL of Tris-HCl buffer (10 mM, pH 8.0)

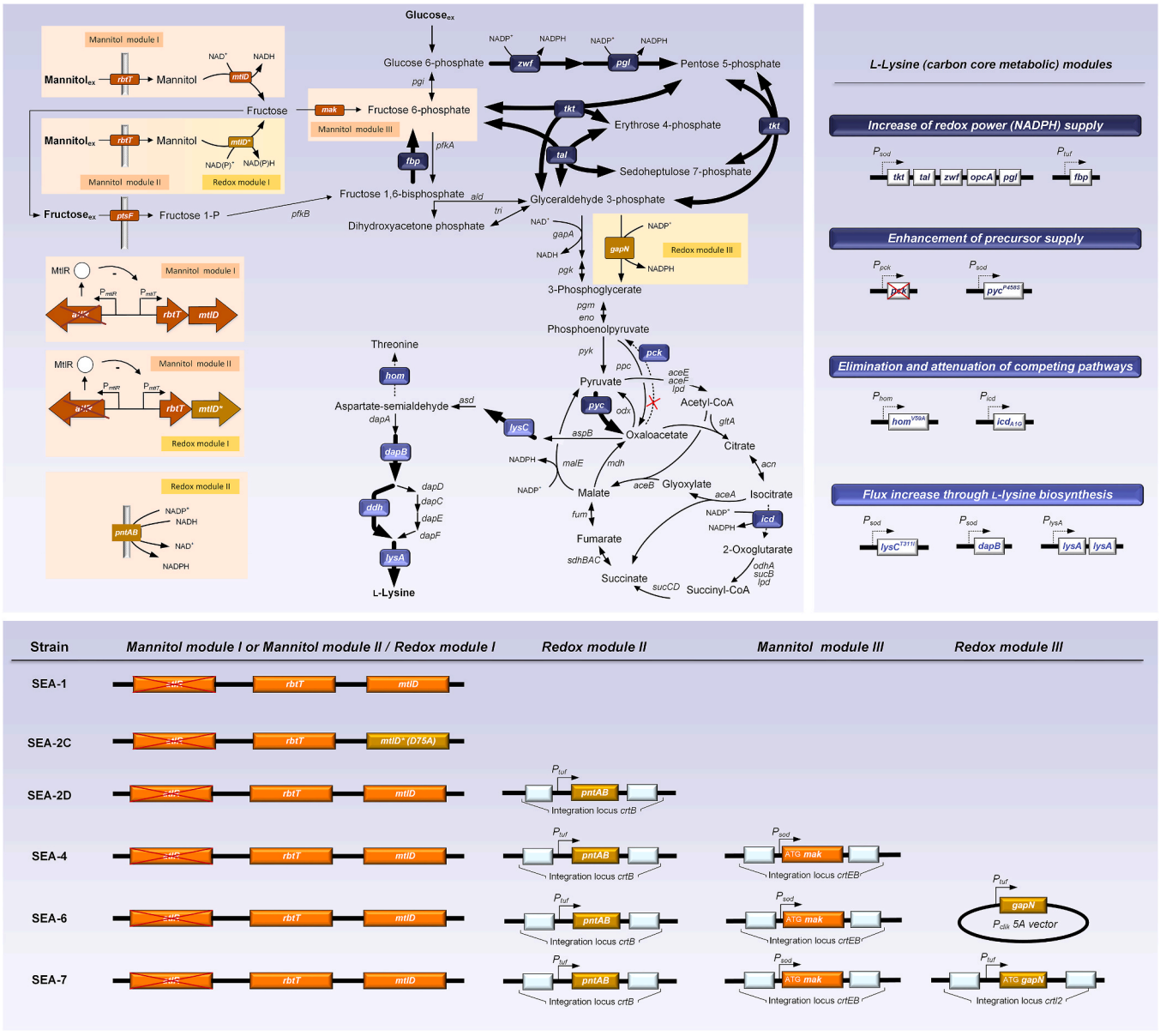

Fig. 1. Metabolic pathway design to produce L-lysine from mannitol in *Corynebacterium glutamicum*. The overview illustrates the genomic layouts of the producers created in this work, including the core carbon metabolism and L-lysine synthesis (blue), mannitol catabolism (orange), and redox metabolism (yellow) pathways. The basic producer SEA-1 served as the starting point for this work (Hoffmann et al., 2018). It was recently established by deletion of the repressor AtlR (also known as MtlR) in *C. glutamicum* LYS-12, which additionally contained twelve genome-based modifications for L-lysine hyperproduction from glucose (shown in blue in the figure) (Becker et al., 2011). The newly created mannitol dehydrogenase variant MtlD D75A partly used NADPH as a cofactor (mannitol module II, redox module I). Expression of *pntAB* from *E. coli*, encoding membrane-bound transhydrogenase, was used to establish redox module II. The gene was integrated under the control of the constitutive *tuf* promoter into the *crtB* locus of *C. glutamicum*. In addition, fructokinase from *E. coli* (*mak*) was inserted into the *crtEb* locus under the control of the constitutive *sod*-promoter (mannitol module III), and NADPH-dependent glyceraldehyde 3-phosphate dehydrogenase was expressed in its native form on an episomal plasmid and in a codon-optimized form under the control of *tuf* integrated into the *crtI2* locus. The gene annotations for central carbon metabolism and L-lysine synthesis are given in the supplementary file 1.

and subsequently resuspended in 0.5 mL of the same buffer. Transhydrogenase activity was analysed at 30 °C in a 1 mL mixture that contained 50 mM potassium phosphate (pH 7.0), 100 mM NaCl, 10 mM β-mercaptoethanol, 0.1 mM NADPH, 0.1 mM 3-acetylpyridine-NAD^+, and 25 μL of resuspended membrane protein solution, via monitoring the increase in absorbance at 375 nm. One unit of activity was defined as the production of 1 μmol of 3-acetylpyridine-NADH per minute. Negative controls were carried out without substrate and cell extract.

All enzyme activities are given as specific activity [U mg^{-1}] correlated to the protein concentration in the extract (Hoffmann et al., 2018).

2.16. Analysis of the cellular redox state

The protocol used to quench intracellular metabolism during sampling was adapted from previous work (Moritz et al., 2000). In short, 5 mL culture broth was mixed with 10 mL pre-cooled methanol (−58 °C, 60% (v/v)) and centrifuged (5 min, 9400×*g*, −10 °C), whereby the temperature of the quenched sample remained below −20 °C. The nicotinamide adenine dinucleotides were immediately extracted from the obtained cell pellet and assayed (EnzyChrom $NAD(P)^+$/NAD(P)H Assay Kit, BioAssay System, Hayward, CA, USA), following the manufacturer's instructions.

2.17. Statistical analysis

For significance analysis, data were subjected to one-way analysis of variance (ANOVA), followed by Fisher's least significant difference (LSD) test and Duncan's multiple range test. Values were considered statistically significant when the P value was less than 0.05 ($P < 0.05$, *) or 0.01 ($P < 0.01$, **). The SPSS 24.0 software (SPSS Inc., Chicago, IL, USA) was used for statistical analysis.

3. Results and discussion

3.1. Mannitol-grown C. glutamicum SEA-1 reveals a perturbed redox metabolism, limited NADPH availability, and excess NAD^+

Intracellular redox levels are important drivers of metabolism. As an example, a sufficient NADPH/$NADP^+$ ratio is crucial for microbial L-lysine production, which has a high demand for NADPH. Here, the recently developed basic L-lysine-producer *C. glutamicum* SEA-1, containing twelve genetic modifications for enhanced L-lysine synthesis and a derepressed mannitol utilization was used as starting point of development (Fig. 1). It was interesting to note that the NADPH/$NADP^+$ ratio of mannitol-grown SEA-1 was severely reduced as compared to glucose-grown cells (Fig. 2). The limited NADPH availability likely explained the much lower L-lysine yield (Table 2) (Becker et al., 2011). The NADH/NAD^+ ratio on mannitol was reduced too. This was surprising on a first glance. Intuitively, one might have expected an increased value due to the stoichiometric formation of NADH in mannitol catabolism (Hoffmann et al., 2018). However, this was not the case, and SEA-1 showed excess NAD^+ on mannitol, even more than on glucose (Fig. 2).

Thermodynamic inspections explained the low NADH/NAD^+ ratio in SEA-1 and unravelled a severe problem, faced by mannitol-grown *C. glutamicum*. At neutral pH (expected for the cytoplasm of *C. glutamicum* during growth at neutral pH as done here) (Follmann et al., 2009; Kelle et al., 1996; Krämer et al., 1990), the oxidation of mannitol to fructose required a large excess of mannitol and NAD^+ over fructose, NADH, and protons, as inferred from the low equilibrium constant ($K_{eq} = 6.2 \times 10^{-9}$) (Voegele et al., 2005). For SEA-1, exhibiting a cytoplasmic pH of 7.0 (Follmann et al., 2009; Kelle et al., 1996; Krämer et al., 1990) and a ratio of NADH/NAD^+ = 0.2 (Figs. 2 and 5A), the intracellular pool of fructose had to be approximately 3-fold lower than the mannitol pool to enable forward operation of MtlD.

However, it appeared possible that mannitol-grown SEA-1 accumulated fructose inside the cells due to its limited fructose conversion capacity. *C. glutamicum* lacks kinases for fructose conversion present in other microbes (Lange et al., 2017) and in plant tissues, where the immediate removal of fructose by glycolysis is regarded as crucial to drive mannitol oxidation (Voegele et al., 2005). Naturally, *C. glutamicum* faces intracellular fructose only during growth on the disaccharide sucrose (from intracellular cleavage of sucrose 6-phosphate to glucose 6-phosphate and fructose), but this growth mode is linked to much weaker generation of sugar in the cytoplasm compared to the synthetic mannitol metabolism created here (Wittmann et al., 2004), while fructose as a substrate enters the cell from the outside as fructose 1-phosphate (via the fructose specific PTS) and a minor proportion of fructose 6-phosphate (via the glucose specific PTS) (Becker et al., 2005; Ikeda, 2012).

Indeed, SEA-1 showed a large intracellular fructose pool (Table S14, supplementary file 1). Moreover, the cells exhibited a rather high cytoplasmic fructose/mannitol ratio (Fig. 5C). As a result, mannitol dehydrogenase unfavourably operated close to equilibrium. The corresponding distance to equilibrium (Γ/K_{eq}), i. e. the ratio between the *in vivo* mass action ratio (Γ) and the equilibrium constant (K_{eq}) was close to 1 (Table 3).

Upon being forced to grow on mannitol, SEA-1 responded in two ways to create an outcome against the disadvantageous thermodynamics: (i) it largely removed fructose by excretion and, *inter alia*, (ii) kept the NADH/NAD^+ ratio low to provide the required driving force. Therefore, the massive fructose secretion by SEA-1 was not caused by

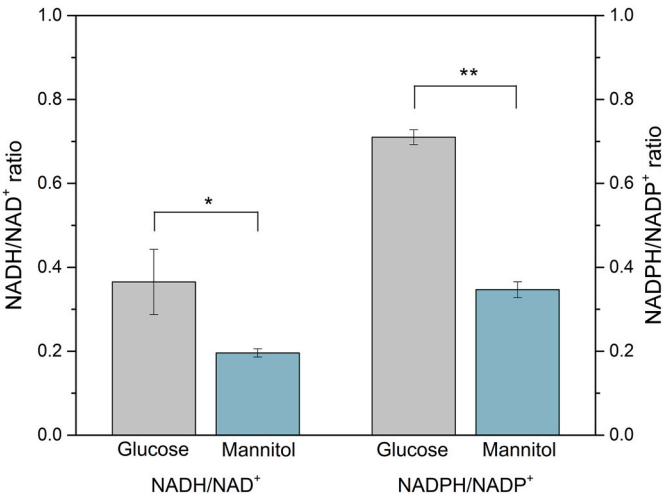

Fig. 2. Redox metabolism in L-lysine producing *C. glutamicum* SEA-1 grown on glucose and mannitol. The samples were taken during exponential growth at OD = 1. Error bars represent standard deviations from three biological replicates (*$p < 0.05$, **$p < 0.01$, NS = not significant).

Table 2
Growth and production performance of L-lysine-producing *C. glutamicum* strains during batch cultivation using mineral salt medium with mannitol as the sole carbon source. The data comprise specific rates for growth (μ_{max}), mannitol uptake (q_{Mtl}), mannitol catabolism ($q_{Mtl,cat}$), and L-lysine formation (q_{Lys}). Additionally, yields for L-lysine ($Y_{Lys/Mtl}$), biomass ($Y_{X/Mtl}$), and fructose ($Y_{Frc/Mtl}$) are given. Errors represent standard deviations of three biological replicates. The data for SEA-1 are taken from previous work and refer to the major phase of cultivation under mannitol excess (Hoffmann et al., 2018).

Strain	SEA-1	SEA-2C
q_{Lys} [mmol g^{-1} h^{-1}]	0.6 ± 0.0	1.0 ± 0.0
q_{Mtl} [mmol g^{-1} h^{-1}]	6.1 ± 1.1	3.7 ± 0.1
$q_{Mtl,cat}$ [mmol g^{-1} h^{-1}]	4.5 ± 1.1	3.7 ± 0.1
μ_{max} [h^{-1}]	0.26 ± 0.00	0.16 ± 0.02
$Y_{Lys/Mtl}$ [mmol mol^{-1}]	90.1 ± 1.1	279.8 ± 18.1
$Y_{Frc/Mtl}$ [mmol mol^{-1}]	262.1 ± 14.2	<0.01
$Y_{X/Mtl}$ [g mol^{-1}]	40.2 ± 2.0	43.1 ± 4.0

Table 3
Thermodynamics of mannitol oxidation to fructose, catalysed by mannitol 2-dehydrogenase in L-lysine producing *C. glutamicum* strains on minimal mannitol medium. The data comprise the *in vivo* mass action ratio (Γ), estimated from the intracellular ratios of NAD/NADH (Fig. 5A), fructose/mannitol (Fig. 5C), and the cytoplasmic pH, the thermodynamic equilibrium constant of mannitol oxidation (K_{eq}) (Voegele et al., 2005), and the distance from the estimated equilibrium (Γ/K_{eq}), calculated as described previously (Wittmann et al., 2005). Samples for intracellular metabolite analysis were taken during exponential growth at OD 1.

Strain	SEA-1	SEA-2C	SEA-2D	SEA-4	SEA-7
K_{eq}	6.20×10^{-9}	6.20×10^{-9}	6.20×10^{-9}	6.20×10^{-9}	6.20×10^{-9}
Γ	6.58×10^{-9}	3.08×10^{-10}	4.15×10^{-9}	5.82×10^{-9}	3.09×10^{-10}
Γ/K_{eq}	1.06	0.05	0.67	0.94	0.05

NADH-related inhibition at the level of glyceraldehyde 3-phosphate, as assumed until recently (Kiefer et al., 2004; Toyoda and Inui, 2016; Yokota and Lindley, 2005). In fact, it was crucial to remove the sugar from the cytoplasm and keep mannitol dehydrogenase in operation. As another bottleneck, SEA-1 supplied NADPH for L-lysine mainly via the TCA cycle due to its low pentose phosphate (PP) pathway flux (Hoffmann et al., 2018), which in turn delivered even more NADH.

Altogether, mannitol-grown *C. glutamicum* SEA-1 exhibited a perturbed redox metabolism and substantial fructose excretion, superimposed by the unfavourable thermodynamics of mannitol oxidation.

3.2. Electrostatic engineering of the catalytic site of mannitol dehydrogenase creates $NADP^+$-dependent activity with high affinity and enhances mannitol-based L-lysine production

The mannitol dehydrogenase MtlD of *C. glutamicum* almost exclusively used NAD^+ as a cofactor (Table 4) and generated undesirable amounts of NADH during mannitol utilization. Considering the NADPH limitation (Fig. 2), a modulation of the cofactor specificity of MtlD appeared promising. For this purpose, a 3D model of the protein structure of MtlD of *C. glutamicum* was constructed using the crystallographic structure of *Pseudomonas fluorescens* MtlD (pdb entry 1M2W.pdb) as the template, since no crystallographic protein structure for MtlD of *C. glutamicum* was available. The template structure revealed 44% sequence identity, suggesting satisfactory predictive power. To identify the position of $NADP^+$, its phosphate substituent was added into the NAD^+-containing crystal structure of the enzyme of *P. fluorescens,* and the exact location of the cofactor was calculated by energy optimization. Based on this layout, the 3D structure of the cofactor-binding pocket of the mannitol dehydrogenase of *C. glutamicum* with bound $NADP^+$ was derived (Fig. 3A, protein data bank (pdb) file, provided as supplementary file 2). Obviously, the negatively charged carboxylate group of Asp75, naturally stabilizing the binding of NAD^+ by bifurcated hydrogen bonds with the adenosyl-ribose ring (Bommareddy et al., 2014), unfavourably repelled the negatively charged phosphate group of $NADP^+$.

Table 4
Kinetic properties of the native mannitol 2-dehydrogenase MtlD and its engineered variant MtlD D75A (MtlD[a]). *C. glutamicum* SEA-1 (MtlD) and SEA-2C (MtlD[a]) were grown on mannitol mineral salt medium at 30 °C. Error bars represent standard deviations of three biological replicates.

Strain	$K_{M,\ NAD}$ (mM)	$V_{max,\ NAD}$ (mU mg^{-1})	$K_{M,\ NADP}$ (mM)	$V_{max,\ NADP}$ (mU mg^{-1})
SEA-1	0.8 ± 0.1	378 ± 15	n.d.[a]	1 ± 0
SEA-2C	1.1 ± 0.1	149 ± 4	0.7 ± 0.1	13 ± 1

[a] Not determined.

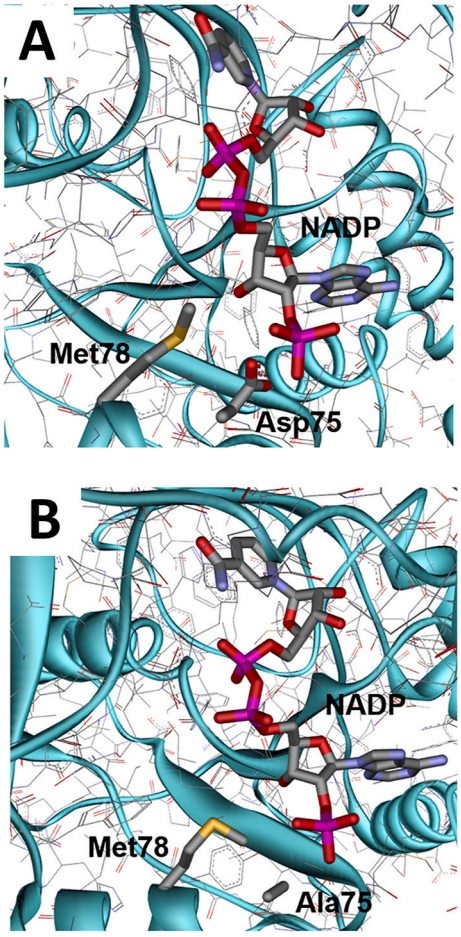

Fig. 3. Homology models of the cofactor-binding site of wild-type NAD^+-specific mannitol 2-dehydrogenase (MtlD) of *C. glutamicum* (A) and a predicted $NADP^+$-dependent mutant MtlD* with the mutation D75A (B), displaying carbon (grey), nitrogen (blue), oxygen (red), phosphorous (pink), and sulphur (yellow). The corresponding protein data base (pdb) file is provided as supplementary file 2.

To avoid this collision, L-aspartate 75 had to be replaced by a rather small amino acid to be able to accommodate the additional phosphate group. By using the Swiss-Pdb Viewer to carry out putative mutations in the homology model, we found out that among the conceivable non-polar amino acids only L-alanine was small enough to avoid steric clashes (Fig. 3B). Due to steric hindrance, larger amino acids containing polar or positively charged side chains to further enhance interactions with the phosphate group could be ruled out as candidates. Accordingly, L-aspartate 75 was replaced by L-alanine in the protein via introduction of the point mutation D75A into the *mtlD* gene (Fig. 3B). The novel strain that expressed MtlD* was designated SEA-2C. Fortunately, the D75A mutant exhibited the desired $NADP^+$-specific activity, and the corresponding conversion rate increased by almost 15-fold, while that for NAD^+ decreased. The mutant enzyme showed even greater affinity for $NADP^+$ than for NAD^+ (Table 4). It should be mentioned that computational modelling predicted a second amino acid exchange in addition to D75A to enhance cofactor specificity for $NADP^+$, that is, replacement of L-methionine by a positively charged L-lysine at the neighbouring position 78 (M78K), which should further support binding of the phosphate group of $NADP^+$ (Fig. 3). However, the double variant was no longer functional; the corresponding mutant no longer grew on mannitol (no strain name assigned; data not shown).

SEA-2C, expressing the single D75A mutant, accumulated 19 mM L-lysine (Fig. S3AB, supplementary file 1) and exhibited a substantially improved production performance compared to the parent strain SEA-1

(Table 2): (i) a more than three-fold higher L-lysine yield, (ii) an almost doubled L-lysine production rate and (iii) elimination of undesired fructose overflow. Interestingly, SEA 2C strongly accumulated intracellular mannitol, which was likely the consequence of the derepressed mannitol influx (caused by the *mtlR* deletion) that could only partially be converted by the mutated enzyme. This scenario *inter alia* resulted in a rather small intracellular fructose pool (Table S14, supplementary file 1) and nicely explained the fact that fructose was not secreted by this strain (Table 3, Fig. S3AB, supplementary file 1). The redox metabolism remained relatively unaffected (Fig. 5).

The specific impact of the changed cofactor preference on metabolic efficiency became obvious, when considering the L-lysine formed from truly *catabolized* mannitol (not secreted as fructose). SEA-1 internalized mannitol at a rate of 4.5 mmol g^{-1} h^{-1} and produced 0.6 mmol L-lysine g^{-1} h^{-1}. Considering only the fraction of catabolized mannitol, SEA-1 exhibited a conversion yield of 0.13 (mol L-lysine) (mol catabolized mannitol)$^{-1}$, while the corresponding value for SEA-2C was more than twice as high, i.e., 0.28 mol mol^{-1}. Altogether, the findings indicated that the introduced $NADP^+$ specificity of MtlD* channelled extra carbon towards L-lysine biosynthesis. The reduced mannitol catabolism, however, appeared as a drawback of the MtlD* mutant.

3.3. Expression of membrane-bound transhydrogenase improves L-lysine production and cellular fitness

Given the perturbed redox levels (Fig. 2) and the previously shown, limited success of heterologous fructose kinase expression to improve the performance of SEA-1 (Hoffmann et al., 2018), membrane-bound transhydrogenase was chosen as the next target. Driven by the proton motive force, the enzyme catalysed a potentially beneficial conversion: the oxidation of NADH to NAD^+ coupled to the reduction of $NADP^+$ to NADPH (Jackson, 2003; Kabus et al., 2007). In line, overexpression of PntAB has been found useful to drive redox-demanding production in other *C. glutamicum* strains (Kabus et al., 2007; Yamauchi et al., 2014; Zhan et al., 2019).

The new strain SEA-2D (SEA-1 P_{tuf} *pntAB*) harboured a genome-based copy of the transhydrogenase gene from *E. coli*. This strain exhibited the desired transhydrogenase activity (497.9 ± 30.8 mU mg^{-1}), whereas SEA-1 did not (<0.1 mU mg^{-1}). When tested in batch culture, SEA-2D accumulated 12.8 mM L-lysine (Fig. S3CD, supplementary file 1), 45% more than SEA-1 (Hoffmann et al., 2018). In addition, SEA-2D formed the product at almost three-fold increased yield and productivity (Table 5). As an additional benefit, secretion of fructose was eliminated, likely supported by a low intracellular fructose level (Table S14, supplementary file 1) and a reduced fructose/mannitol ratio that provided extra driving force for mannitol oxidation (Fig. 5C, Table 3).

From the viewpoint of kinetics, SEA-2D was superior to the MtlD* mutant SEA-2C. It grew 30% faster (Table 2, Table 5) and completed the entire cultivation in only two-thirds of the time (Fig. S3CD, supplementary file). In addition, SEA-2D used 20% more carbon for growth, indicating its significantly better fitness. Regarding production stoichiometry, however, SEA-2D was not as efficient: its L-lysine yield was slightly lower than that of SEA-2C (Table 2, Table 5).

To understand in more detail how the expression of PntAB affected the metabolism of *C. glutamicum,* the SEA-2D mutant was analysed at the metabolic flux level using a ^{13}C-based approach for mannitol-grown *C. glutamicum*; this method was recently developed (Hoffmann et al., 2018) and extended here to additionally estimate fluxes through malic enzyme and the novel PntAB transhydrogenase, considering *in vitro* activities of the enzymes as constraints and consistency checks (Lange et al., 2017). The approach provided a distribution of intracellular carbon fluxes through the metabolism of *C. glutamicum* SEA-2D (Fig. 4A).

SEA-2D channelled more than 90% of the utilized substrate via fructose 1-phosphate and fructose 1,6-bisphosphate towards the lower Emden-Meyerhof-Parnas (EMP) pathway. The PP pathway exhibited a minor flux of 5% and contributed only a small amount of reducing power (10% flux, 15-fold less than that on glucose (Becker et al., 2011)). Despite the low supply from this commonly regarded major NADPH supply route, SEA-2D channelled a high flux of 24% through the L-lysine pathway, with other pathways contributing to supply redox power. The TCA cycle generated the highest amount of NADPH (isocitrate dehydrogenase flux of 78%), and malic enzymes supplied NADPH as well (23%), which matched well with the determined *in vitro* activity of 158 mU mg^{-1} as an upper constraint (Table S10, supplementary file 1). Notably, the newly introduced transhydrogenase carried a flux of 66%, making it the second most important enzyme to supply NADPH in SEA-2D and underlining its beneficial impact on L-lysine production.

Table 5
Growth and production of L-lysine-producing *C. glutamicum* strains during batch cultivation in shake flasks using mineral mannitol medium (Fig. S4A-F, supplementary file 1). The data comprise specific rates for growth (μ_{max}), mannitol uptake (q_{Mtl}), mannitol catabolism ($q_{Mtl,cat}$), and L-lysine formation (q_{Lys}). Additionally, yields for L-lysine ($Y_{Lys/Mtl}$), biomass ($Y_{X/Mtl}$), and fructose ($Y_{Frc/Mtl}$) are given. The data represent the entire cultivation for SEA-2D, SEA-6, and SEA-7. For the fructose-accumulating strains SEA-4 and SEA-5, the data reflect the major phase under mannitol excess (shown in white for SEA-4 in Fig. S4AB, supplementary file 1). Data on additional by-products are shown in Table S3 (**supplementary file 1**). Errors represent standard deviations of three biological replicates.

Strain	SEA-2D	SEA-4	SEA-5	SEA-6	SEA-7
q_{Lys} [mmol g^{-1} h^{-1}]	0.91 ± 0.04	0.85 ± 0.01	0.84 ± 0.02	1.59 ± 0.03	1.58 ± 0.05
q_{Mtl} [mmol g^{-1} h^{-1}]	4.0 ± 0.1	5.4 ± 0.3	5.2 ± 0.2	5.1 ± 0.1	5.3 ± 0.1
$q_{Mtl,cat}$ [mmol g^{-1} h^{-1}]	4.0 ± 0.1	4.4 ± 0.3	4.0 ± 0.2	5.1 ± 0.1	5.3 ± 0.1
μ_{max} [h^{-1}]	0.21 ± 0.01	0.29 ± 0.03	0.24 ± 0.06	0.24 ± 0.02	0.25 ± 0.02
$Y_{Lys/Mtl}$ [mmol mol^{-1}]	224.9 ± 5.0	159.3 ± 8.1	163.3 ± 9.1	311.9 ± 7.6	299.5 ± 4.8
$Y_{Frc/Mtl}$ [mmol mol^{-1}]	<0.01	179.3 ± 8.7	239.9 ± 13.4	<0.01	<0.01
$Y_{X/Mtl}$ [g mol^{-1}]	52.0 ± 3.9	53.5 ± 1.8	45.9 ± 9.3	47.2 ± 3.0	47.8 ± 5.4

While mannitol catabolism functioned well and L-lysine formation was substantially enhanced in SEA-2D, the high TCA cycle flux remained a bottleneck, given the undesirable excess loss of carbon resulting from the generation of NADPH via the cycle compared to the other pathways. It was interesting to note that the redox ratios remained rather unaffected by the expression of PntAB (Fig. 5AB). Despite the improved L-lysine production, the availability of NADPH and the NADH/NAD^+ ratio were still at low levels. Obviously, the vital contribution of PntAB did not fully restore the redox imbalance, indicating room for further improvement.

3.4. C. glutamicum SEA-7 exhibits a debottlenecked carbon core metabolism and forms L-lysine from mannitol at 30% molar yield

The second-generation strain SEA-2D exhibited excellent production capacity and high vitality and was therefore chosen as the chassis to further enhance performance. SEA-2D still exhibited a perturbed redox state, so further rounds of strain engineering aimed at resolving this issue. A first modification introduced the fructokinase Mak from *E. coli*, suggested recently to enhance the PP pathway flux on mannitol, although the resulting benefits (at the level of SEA-1) were found only minor (Hoffmann et al., 2018). However, it appeared promising to implement and test this modification in SEA-2D, given also the beneficial properties of overexpressing fructokinase in other *C. glutamicum* strain backgrounds and on other substrates (Xu et al., 2013, 2020; Zhang et al., 2017). The corresponding mutant SEA-4 produced more L-lysine than SEA-2D (Fig. S3CD; Fig. S4AB, supplementary file 1). Its specific L-lysine production rate was increased by 54%, which was likely linked

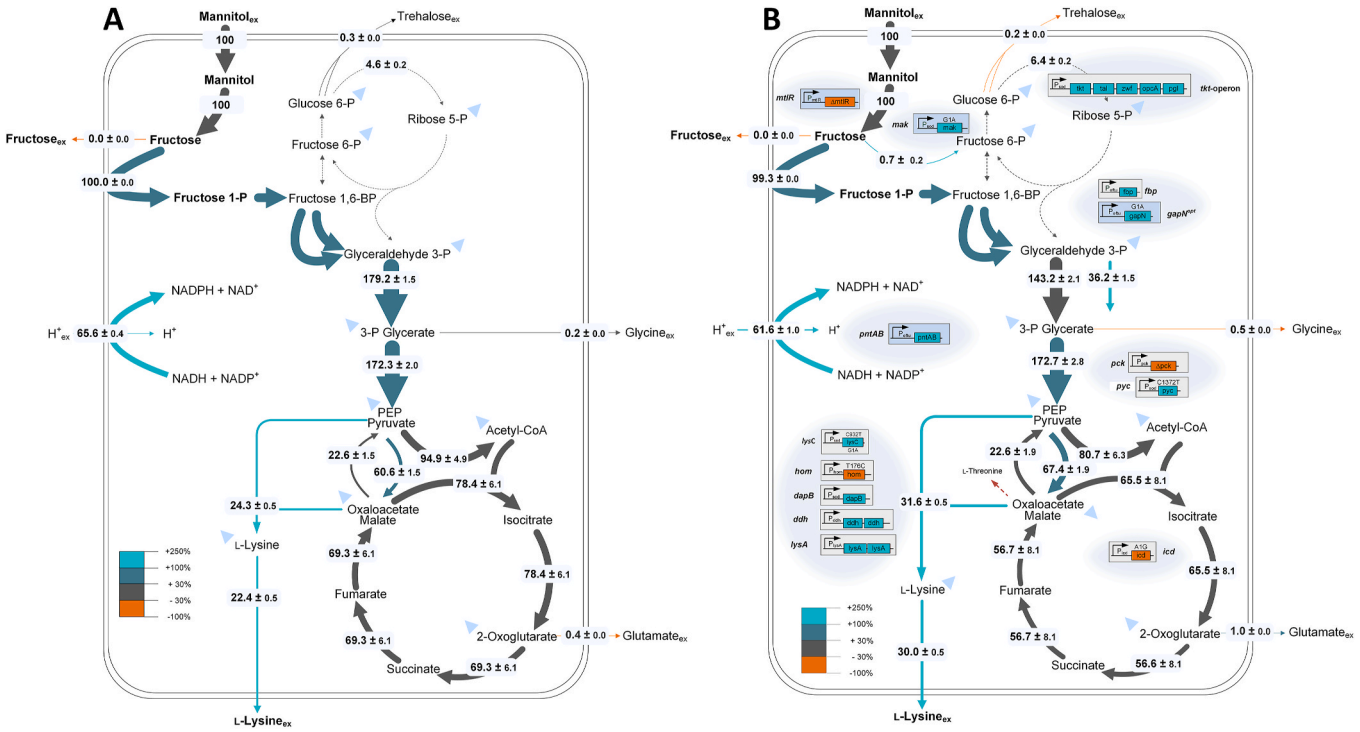

Fig. 4. Intracellular carbon fluxes of mannitol-grown *Corynebacterium glutamicum* SEA-2D (A) and SEA-7 (B), determined by ^{13}C metabolic flux analysis. All fluxes are given as a molar percentage of the mean specific mannitol uptake rate of $q_{Mtl} = 4.0$ mmol g^{-1} h^{-1} (SEA-2D) and $q_{Mtl} = 5.3$ mmol g^{-1} h^{-1} (SEA-7), respectively, which was set to 100%. The reactions for conversion to biomass are indicated as blue triangles. All flux values are given in Tables S4-S13 (supplementary file 1). In addition, all genome-based modifications implemented into the SEA-7 are shown (B).

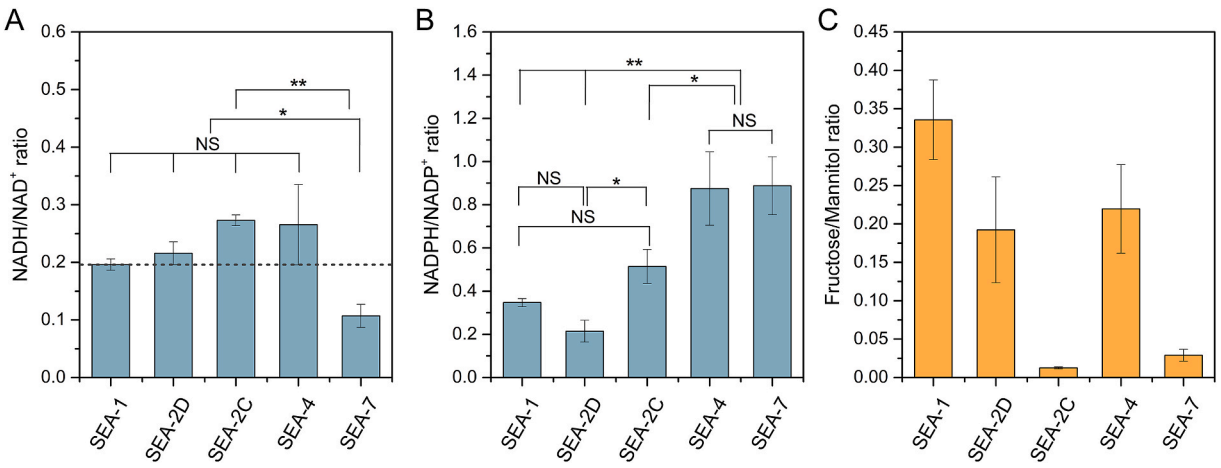

Fig. 5. Redox metabolism (A–B) and ratio of intracellular carbohydrates (C) in l-lysine-producing *C. glutamicum* strains on mannitol. Samples for analysis were taken during exponential growth at OD = 1. Error bars represent standard deviations from three biological replicates (*p < 0.05, **p < 0.01, NS = not significant).

to the improved NADPH availability (Fig. 5B). However, SEA-4 again secreted fructose during the initial culture phase, as the higher influx of mannitol obviously surpassed the catabolization potential of the cells (Fig. S4AB, supplementary file 1) and mannitol dehydrogenase was set back to near-equilibrium operation (Table 3).

Next, non-phosphorylating NADP$^+$-dependent glyceraldehyde 3-phosphate dehydrogenase from *Streptococcus mutans* (Crow and Wittenberger, 1979; Takeno et al., 2010) was implemented due to its recently discovered benefits to provide extra NADPH in mannitol-grown *C. glutamicum* (Hoffmann et al., 2018) and other *C. glutamicum* cell factories (Takeno et al., 2010, 2016). For test purposes, *gapN* was first expressed from an episomal plasmid under the control of its native promoter. Transformation of the corresponding plasmid pClik 5a MCS *gapN* into SEA-4 created strain SEA-6. SEA-6 exhibited substantial NADP$^+$-dependent glyceraldehyde 3-phosphate dehydrogenase activity (250 ± 11 mU mg^{-1}), whereas the parent strain SEA-4 did not (<0.1 mU mg^{-1}). The novel mutant accumulated substantially higher levels of L-lysine (Fig. S4CD, supplementary file 1), thereby achieving an almost doubled product yield (312 mmol mol^{-1}) and an almost doubled specific production rate compared to SEA-4 and surpassing the initial strain SEA-1 in performance by 3.5-fold and 2.6-fold (Table 2, Table 5). Notably, fructose accumulation was completely abolished by GapN expression. Since the control strain SEA-5, harbouring only the empty plasmid, did not exhibit such improvement but matched the characteristics of the ancestor strain (Table 5), the enhanced performance could be fully attributed to the GapN enzyme.

A final round of engineering replaced the plasmid-based *gapN* gene with a genome-based copy to obtain a fully genome-engineered strain. To compensate for the fact that genomic *gapN* would occur only as a single copy compared to multiple copies of a plasmid-based gene, the expression efficiency was tuned. First, the *gapN* sequence was adapted to the preferred codon usage of *C. glutamicum* (Fig. S5, supplementary file 1). Second, the translational start codon of *gapN* (GTG) was replaced by the more common and stronger variant ATG to promote translational efficiency (Becker et al., 2010). Third, the native promoter was replaced by the *tuf* promoter for high expression efficiency in *C. glutamicum* (Becker et al., 2005). *C. glutamicum* SEA-7, obtained after the second recombination, revealed the desired $NADP^+$-dependent GapN activity (462.6 ± 2.4 mU mg^{-1}), almost twice as high as that of the native plasmid-based version. SEA-7 consumed mannitol within only 20 h, much faster than all other strains (Fig. S4, supplementary file 1). Regarding production performance, strain SEA-7 appeared to be as good as the plasmid-based variant (Table 5).

Metabolic flux analysis of SEA-7 revealed high glycolytic activity, supported by the additional GapN, which contributed 36% to the total EMP pathway flux (Fig. 4B). SEA-7 achieved the highest flux towards NADPH among all strains (199%). Isocitrate dehydrogenase (66%), PntAB (62%), GapN (36%), and malic enzyme (23%) were the major NADPH contributors, while carbon flux and redox supply from the PP pathway were low (6% and 12%, respectively). SEA-7 (and its plasmid-based counterpart SEA-6) achieved the best catabolization rates for mannitol of all strains (Table 5), even reaching the high level of glucose catabolization in L-lysine hyperproducers (Becker et al., 2007, 2011).

Interestingly, SEA-7 revealed a beneficially restored redox level (Fig. 5AB), including increased NADPH availability and reduced excess NAD^+. The latter was a clear response to the artificially increased capacity to channel fructose towards central metabolism, which decreased the intracellular level of the sugar (Table S14, supplementary file 1) so that the high NAD^+ excess as a thermodynamic driving force for MtlD was no longer needed (Table 3).

3.5. *C. glutamicum SEA-7 performs well under fed-batch conditions and accumulates 76 g L^{-1} L-lysine from mannitol within 35 h*

To assess performance under more industrially relevant conditions, we benchmarked the SEA-7 strain in a fed-batch process (Fig. 6). During the batch phase, the strain grew exponentially (Fig. 6A) and accumulated L-lysine at a yield of 0.21 mol mol^{-1} (Fig. 6B, Phase I). Thereby, fructose accumulation was observed, which peaked at approximately 14 g L^{-1}, indicating a bottleneck when high levels of mannitol were provided. After 6 h, the initially supplied mannitol (41 g L^{-1}) was depleted, and the feed phase was started. Mannitol was added pulse-wise so that the substrate was kept in a range of 5–10 g L^{-1}. The L-lysine concentration continually increased from 5 g L^{-1} at the end of the batch phase to 32 g L^{-1} after 17 h, providing a product yield of 0.26 mol mol^{-1} (Fig. 6B, Phase II). During this phase, fructose was fully re-consumed.

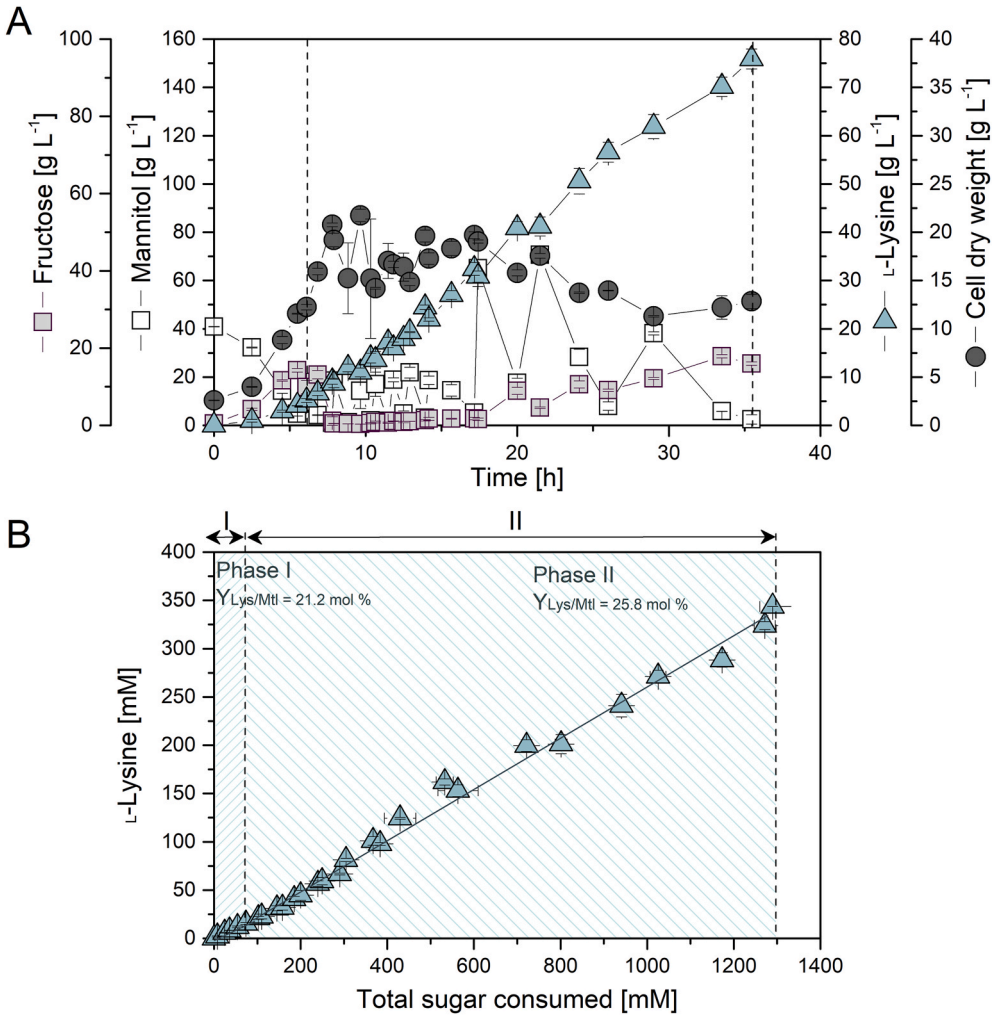

Fig. 6. Fed-batch production of L-lysine by metabolically engineered *C. glutamicum* SEA-7: culture profile (A) and product yield (B). The data represent mean values and deviations from two replicates.

Obviously, *C. glutamicum* SEA-7, equipped with efficient pathways to metabolize mannitol, handled the substrate very well, including at the high starting concentration chosen. Due to the lower solubility of mannitol (216 g L^{-1}), compared to other sugars, the feed was less concentrated, so the reactors had approached their maximum filling capacity. Because SEA-7 was still performing well at this point, the feed was switched, adding solid mannitol every few hours. Each single dose increased the mannitol level by 50 g L^{-1}, and the substrate was then consumed within a short time. Addition of feed was stopped after 29 h to allow depletion of the remaining carbon. The L-lysine level increased to a final titre of 76 g L^{-1} after 35 h. The short cultivation time was comparable to that of the molasses-based fed-batch processes of *C. glutamicum* (Becker et al., 2011). The space-time yield for L-lysine was maximal during the feed phase (2.1 g L^{-1} h^{-1}). Averaged over the full process, production occurred at more than the half-maximum rate (1.5 g L^{-1} h^{-1}). The cells produced L-lysine exclusively. Lactate transiently accumulated as the only by-product but was completely re-consumed later (Fig. S6, supplementary file 1), whereas trehalose levels remained nonsignificant (<0.1 g L^{-1}). The created SEA-7 cell factory exhibited high synthetic selectivity, a strong benefit for downstream processing.

3.6. Cascaded valorization of *L. digitata* to alginate and L-lysine using optimized *C. glutamicum* SEA-7

L. digitata is a major seaweed used for the manufacturing of commercial alginate, a high-value polymer for the food, cosmetic, and pharmaceutical industries due to its superior gelling, thickening and stabilization properties (Fertah et al., 2017; Torres et al., 2019).

Here, ground *L. digitata* powder was treated with hot water, yielding extracts with mannitol as the major sugar (Fig. S7A, supplementary file 1) and smaller shares of L-alanine, L-glutamate, and L-aspartate, the most abundant amino acids in algal biomass (Hou et al., 2015; Manns et al., 2017). Enzymatic hydrolysis conducted after the extraction, additionally provided significant amounts of glucose and fructose and even additional mannitol, resulting from degradation of the *L. digitata* polymer laminarin (Fig. S7B, supplementary file 1) (Hou et al., 2017; Kim et al., 2011). The obtained extracts were quite viscous due to the presence of alginate (Chades et al., 2018; Hou et al., 2015). Alginate was precipitated, followed by several steps of decolorization and purification, which finally yielded pure sodium alginate as a clean, white gum (Fig. 7).

The seaweed extract, remaining after alginate separation, was filtered, and concentrated approximately seven-fold by heating to 70 °C under vacuum. The treatment provided a sugar-rich feed containing high levels of mannitol (53–75 g L^{-1}), glucose (16–22 g L^{-1}) and fructose (0.5–3.5 g L^{-1}) for different *L. digitata* batches, linked to seasonal and regional fluctuations in the sugar content in seaweed (Schiener et al., 2015).

SEA-7 performed well on the mannitol-, glucose-, and fructose-containing hydrolysate (Fig. 8). Its specific growth rate (0.36 h^{-1}) was significantly higher than that on pure mannitol (Table 5) and even reached the value obtained for wild-type *C. glutamicum* on glucose (Becker et al., 2011). The high vitality of SEA-7 was obviously supported by growth-promoting ingredients in the seaweed extract (Torres et al., 2019) and synergistic effects, eventually resulting from co-consumption of the sugars. The sugars represented 95–98% of depolymerized organics. In addition, minor shares of amino acids (mainly L-glutamate, L-alanine, and L-aspartate) were observed (Fig. S7, supplementary file 1). On a quantitative basis, they displayed the remaining fraction of 2–5%, while organic acids and other organics were not detected. Considering these substrates together, SEA-7 produced L-lysine from the residual *L. digitata* stream at a yield of 0.24 C-mol C-mol^{-1}, almost as high as from pure mannitol medium (Fig. 9B). Additional studies using *L. digitata* extracts, directly derived from hot water extraction were also converted by SEA-7 and even resulted in a L-lysine yield of 0.27 C-mol C-mol^{-1} and faster growth than on pure mannitol (Fig. 9, Fig. S8, supplementary file 1).

3.7. Valorization of a commercial waste stream from food processing of the brown seaweed *Durvillaea antarctica* using SEA-7

The large brown seaweed *D. antarctica* is an endemic species of the Southern Hemisphere (Lizée-Prynne et al., 2016; Mansilla et al., 2012, 2017). In Chile, it is collected for food purposes from wild habitats. Commercialization of *D. antarctica* has increased by more than 400% over recent years, reached a production volume of 8000 tons (Ferdouse et al., 2018) and enabled international trading with other countries (Uribe et al., 2018). The soft fronds (blades) of seaweed are processed for human consumption, leaving the rest as a significant waste (Fig. S9AB, supplementary file 1). Extraction of this waste (holdfasts and harder parts of the blades), this time using acid treatment, yielded a hydrolysate containing mannitol, glucose, fructose, and small amounts of galactose (Fig. S7C, supplementary file 1). SEA-7 converted the

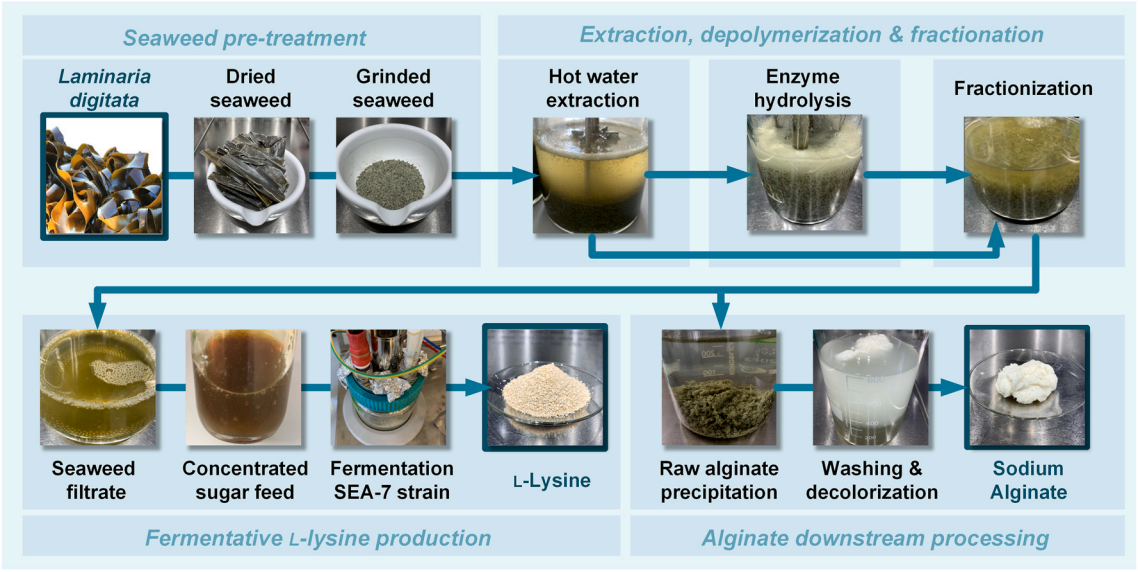

Fig. 7. Cascaded valorization of the industrial seaweed *L. digitata* to alginate and L-lysine using *C. glutamicum* SEA-7, optimized by systems metabolic engineering.

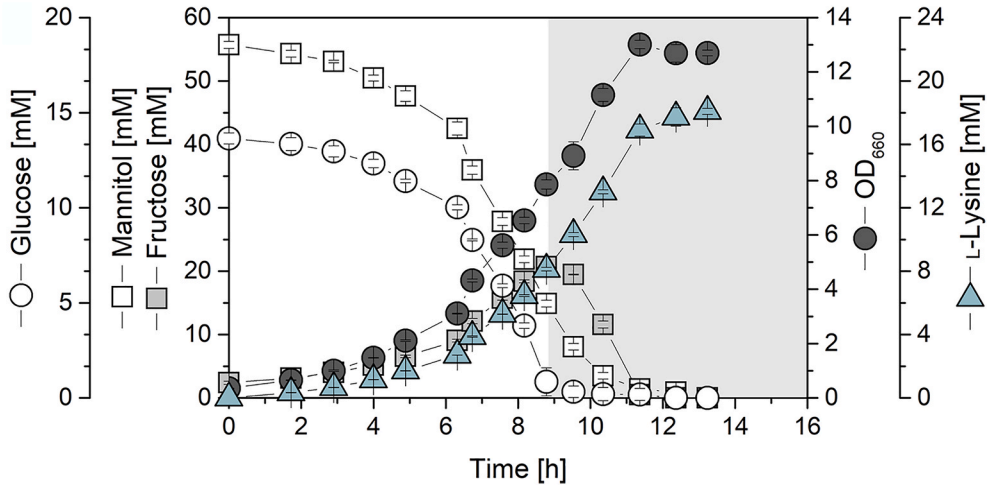

Fig. 8. Production performance of optimized *C. glutamicum* SEA-7 on a sugar-rich hydrolysate of *L. digitata*, obtained as residue after extraction and purification of alginate. The data represent mean values and deviations of three replicates.

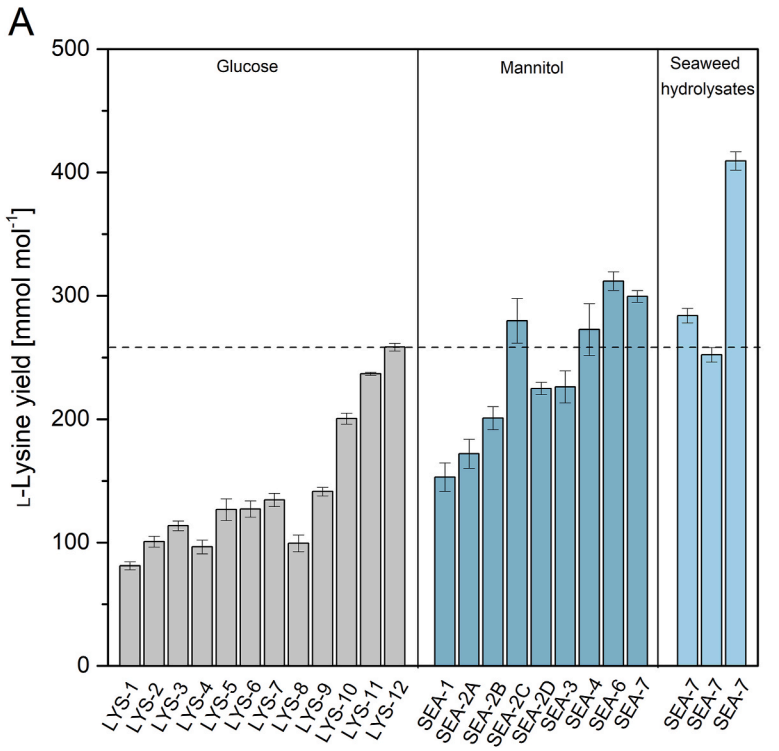

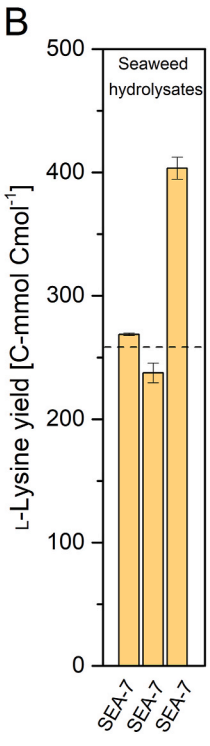

Fig. 9. Benchmarking of tailormade L-lysine-producing strains of *C. glutamicum*: LYS-1 to LYS-12 on glucose (Becker et al., 2011); SEA-1, SEA-2A, SEA-2B, and SEA-3 on mannitol (Hoffmann et al., 2018); SEA-2C, SEA-2D, and SEA-4 to SEA-7 on mannitol (this work) (A), and SEA-7 on seaweed extracts (this work) (A, B). The data display mean values and deviations from three replicates. The calculation of the L-lysine yield on seaweed hydrolysates (B) considered depolymerized organics, present in the complex materials. In addition to total sugar (sum of glucose, fructose, mannitol, contributing approximately 95–98% of carbon on a C-molar basis), bioavailable carbon included smaller amounts of amino acids (mainly L-glutamate, L-alanine, L-aspartate) that were present in the extracts and contributed approximately 2–5% of carbon on a C-molar basis), whereas other organics such as organic acids were not detected. Slightly lower values were derived for the L-lysine yield on seaweed hydrolysates, when only the sugars (sum of glucose, fructose, mannitol) were considered, suggesting that these compounds were the major carbon sources.

useable carbohydrates (galactose was not used) and minor shares of amino acids to L-lysine at a yield of 0.40 C-mol per C-mol^{-1} (Fig. 9B), proving its suitability to valorise commercial seaweed waste. SEA-7 grew slower than on the *L. digitata* hydrolysate (Fig. S8, supplementary file 1), likely due to the increased level of salt originating from pretreatment of the seaweed with sulphuric acid. Similarly, SEA-7 revealed weaker performance on acid hydrolysates obtained from *L. digitata* using HCl (data not shown), suggesting that milder pretreatment strategies should be applied to achieve increased bioavailability in the future.

4. Conclusions

The use of more sustainable raw materials is one of the most relevant tasks to achieve a greener production. Admittedly, biotechnology still largely relies on first and second-generation renewables. As an example L-lysine, a premium feed additive, is primarily manufactured from starch, raw sugar and molasses (Becker et al., 2005, 2011; Gopinath et al., 2011; Hirao et al., 1989; Ikeda, 2017; Seibold et al., 2006; Tateno et al., 2007a, 2007b; Xu et al., 2018). In this work, we established *C. glutamicum* as a production host for the feed amino acid L-lysine from seaweed biomass. For maximized sustainability, the microbe used low-value residual seaweed streams, left over after extraction of the high-value ingredient alginate and the recovery of edible parts for food manufacturing. SEA-7 accumulated forty-fold more L-lysine from mannitol, the major seaweed sugar, than any other microbe engineered to date (Hoffmann et al., 2018).

More work seems, however, needed regarding fermentation strategies. As example, a better control of the mannitol level during fermentation promises higher product yields. Moreover, the less concentrated

mannitol-based feeds will require higher reactor volumes than the ones presently used for conventional sugars. The addition of solid mannitol (as done here to benchmark the strain) is not expected to be preferred for actual production.

Notably, the excellent performance of SEA-7 was enabled by a systematically streamlined metabolism, which included 16 genomic traits that covered the entire route from substrate to product: the L-lysine module (12 genomic changes in 4 different carbon core metabolic modules) to drive L-lysine formation, mannitol modules I and III (2 genomic changes) to drive mannitol uptake, redox module II (1 genomic change) to supply NADPH from NADH, and redox module III to couple the high glycolytic flux further to NADPH supply (Figs. 1 and 4B). In this way, mannitol, a non-natural substrate for *C. glutamicum*, could be efficiently converted to L-lysine, providing an even higher yield than glucose, the gold standard of fermentation (Fig. 9), and enabling efficient production independent of redox supply via the PP pathway (Fig. S4EF, supplement).

Further optimization can be expected by additional rounds of strain engineering (Campbell et al., 2017; Lange et al., 2017; Lynch, 2016; Nielsen, 2017) to complement the use of terrestrial crops for fermentation (Becker et al., 2011; Ikeda et al., 2009; Lee and Park, 2010; Ohnishi et al., 2002) by seaweed biomass from rapidly growing ocean farms. From the point of substrate utilization, metabolic engineering could aim at extending the substrate spectrum of *C. glutamicum* towards alginate, since the structural polysaccharide is abundant in many brown algae species (Kawai and Murata, 2016; Wei et al., 2013). Simultaneous utilization of alginate and mannitol could also be interesting from the fact that the catabolism of alginate requires NADH, which is provided by the oxidation of mannitol (Wargacki et al., 2012). Furthermore, the substrate spectrum of *C. glutamicum* SEA-7 could be expanded by considering other algae species as raw material, such as red algae, since these contain a higher carbohydrate content than brown algae, that can range up to 84% of their dry weight (Wei et al., 2013), which can be broken down into glucose, mannose, and galactose by acid treatment and enzymatic saccharification (Kim et al., 2011). Besides carbohydrates, macroalgae have a large repertoire of hydrocolloids, vitamins, fatty acids, proteins and amino acids, minerals and pigments (Torres et al., 2019), suggesting a cascaded biorefinery to fully harness all valuable compounds while reducing the amount of waste produced (Torres et al., 2019; van Hal et al., 2014). By using such a biorefinery approach, a more sustainable and thus economically more efficient production of industrially important products can be achieved (Poblete-Castro et al., 2020; Torres et al., 2019; van Hal et al., 2014). The production of L-lysine from residual seaweed sugars could display one vital element of such an ocean based sustainable bio-production. In addition, given its excellent L-lysine production performance, SEA-7 could be modified for the production of other commercially attractive compounds which are derived via the L-lysine pathway, such as ectoine (Becker et al., 2013; Gießelmann et al., 2019), 1,5-diaminopentane (Kind et al., 2014), 5-aminovalerate (Rohles et al., 2016), and glutarate (Rohles et al., 2016, 2018), promising additional potential.

Author statement

Sarah Hoffmann, Michael Kohlstedt, Lukas Jungmann, Michael Hutter, Ignacio Poblete-Castro: Investigation, formal analysis, visualization; Sarah Hoffmann, Judith Becker, Christoph Wittmann: Drafting the manuscript; Judith Becker, Christoph Wittmann: Design of study, supervision, review & editing; Christoph Wittmann: Conceptualization, resources, funding acquisition.

Declaration of competing interest

There are no conflicts to declare.

Acknowledgements

The authors acknowledge the excellent assistance provided by Michel Fritz for analytics. This study received funding from the German Research Foundation (Grant no. INST 256/418-1), the Federal Ministry of Education and Research (EXPLOMARE, Grant no. 161B0868D), and the Hans&Ruth-Giessen-Stiftung.

Appendix A. Supplementary data

Supplementary data to this article can be found online at https://doi.org/10.1016/j.ymben.2021.07.010.

References

Adams, J.M.M., Toop, T.A., Donnison, I.S., Gallagher, J.A., 2011. Seasonal variation in *Laminaria digitata* and its impact on biochemical conversion routes to biofuels. Bioresour. Technol. 102, 9976–9984. https://doi.org/10.1016/j.biortech.2011.08.032.

Alaswad, A., Dassisti, M., Prescott, T., Olabi, A.G., 2015. Technologies and developments of third generation biofuel production. Renew. Sustain. Energy Rev. 51, 1446–1460. https://doi.org/10.1016/j.rser.2015.07.058.

Anusree, M., Wendisch, V.F., Nampoothiri, K.M., 2016. Co-expression of endoglucanase and β-glucosidase in *Corynebacterium glutamicum* DM1729 towards direct lysine fermentation from cellulose. Bioresour. Technol. 213, 239–244. https://doi.org/10.1016/j.biortech.2016.03.019.

Balat, M., 2011. Production of bioethanol from lignocellulosic materials via the biochemical pathway: a review. Energy Convers. Manag. 52, 858–875. https://doi.org/10.1016/j.enconman.2010.08.013.

Becker, J., Buschke, N., Bücker, R., Wittmann, C., 2010. Systems level engineering of *Corynebacterium glutamicum*–Reprogramming translational efficiency for superior production. Eng. Life Sci. 10, 430–438. https://doi.org/10.1002/elsc.201000008.

Becker, J., Klopprogge, C., Herold, A., Zelder, O., Bolten, C.J., Wittmann, C., 2007. Metabolic flux engineering of L-lysine production in *Corynebacterium glutamicum* - over expression and modification of G6P dehydrogenase. J. Biotechnol. 132, 99–109. https://doi.org/10.1016/j.jbiotec.2007.05.026.

Becker, J., Klopprogge, C., Zelder, O., Heinzle, E., Wittmann, C., 2005. Amplified expression of fructose 1,6-bisphosphatase in *Corynebacterium glutamicum* increases in vivo flux through the pentose phosphate pathway and lysine production on different carbon sources. Appl. Environ. Microbiol. 71, 8587–8596. https://doi.org/10.1128/AEM.71.12.8587-8596.2005.

Becker, J., Schäfer, R., Kohlstedt, M., Harder, B.J., Borchert, N.S., Stöveken, N., Bremer, E., Wittmann, C., 2013. Systems metabolic engineering of *Corynebacterium glutamicum* for production of the chemical chaperone ectoine. Microb. Cell Factories 12, 110. https://doi.org/10.1186/s12934-016-0553-0.

Becker, J., Wittmann, C., 2012. Systems and synthetic metabolic engineering for amino acid production – the heartbeat of industrial strain development. Curr. Opin. Biotechnol. 23, 718–726. https://doi.org/10.1016/j.copbio.2011.12.025.

Becker, J., Zelder, O., Häfner, S., Schröder, H., Wittmann, C., 2011. From zero to hero - design-based systems metabolic engineering of *Corynebacterium glutamicum* for L-lysine production. Metab. Eng. 13, 159–168. https://doi.org/10.1016/j.ymben.2011.01.003.

Benkert, P., Biasini, M., Schwede, T., 2011. Toward the estimation of the absolute quality of individual protein structure models. Bioinformatics 27, 343–350. https://doi.org/10.1093/bioinformatics/btq662.

Bommareddy, R.R., Chen, Z., Rappert, S., Zeng, A.-P., 2014. A *de novo* NADPH generation pathway for improving lysine production of *Corynebacterium glutamicum* by rational design of the coenzyme specificity of glyceraldehyde 3-phosphate dehydrogenase. Metab. Eng. 25, 30–37. https://doi.org/10.1016/j.ymben.2014.06.005.

Buschke, N., Becker, J., Schäfer, R., Kiefer, P., Biedendieck, R., Wittmann, C., 2013a. Systems metabolic engineering of xylose-utilizing *Corynebacterium glutamicum* for production of 1,5-diaminopentane. Biotechnol. J. 8, 557–570. https://doi.org/10.1002/biot.201200367.

Buschke, N., Schäfer, R., Becker, J., Wittmann, C., 2013b. Metabolic engineering of industrial platform microorganisms for biorefinery applications–optimization of substrate spectrum and process robustness by rational and evolutive strategies. Bioresour. Technol. 135, 544–554. https://doi.org/10.1016/j.biortech.2012.11.047.

Buschke, N., Schröder, H., Wittmann, C., 2011. Metabolic engineering of *Corynebacterium glutamicum* for production of 1,5-diaminopentane from hemicellulose. Biotechnol. J. 6, 306–317. https://doi.org/10.1002/biot.201000304.

Campbell, K., Xia, J., Nielsen, J., 2017. The impact of systems biology on bioprocessing. Trends Biotechnol. 35, 1156–1168. https://doi.org/10.1016/j.tibtech.2017.08.011.

Chades, T., Scully, S.M., Ingvadottir, E.M., Orlygsson, J., 2018. Fermentation of mannitol extracts from brown macro algae by thermophilic *Clostridia*. Front. Microbiol. 9 https://doi.org/10.3389/FMICB.2018.01931, 1931-1931.

Chen, Z., Liu, G., Zhang, J., Bao, J., 2019. A preliminary study on L-lysine fermentation from lignocellulose feedstock and techno-economic evaluation. Bioresour. Technol. 271, 196–201. https://doi.org/10.1016/j.biortech.2018.09.098.

Cheng, J., Chen, P., Song, A., Wang, D., Wang, Q., 2018. Expanding lysine industry: industrial biomanufacturing of lysine and its derivatives. J. Ind. Microbiol. Biotechnol. 45, 719–734. https://doi.org/10.1007/s10295-018-2030-8.

Crow, V.L., Wittenberger, C.L., 1979. Separation and properties of NAD^+- and $NADP^+$-dependent glyceraldehyde-3-phosphate dehydrogenases from *Streptococcus mutans*. J. Biol. Chem. 254, 1134–1142. https://doi.org/10.1016/S0021-9258(17)34179-0.

Eggeling, L., Bott, M., 2015. A giant market and a powerful metabolism: L-lysine provided by *Corynebacterium glutamicum*. Appl. Microbiol. Biotechnol. 99, 3387–3394. https://doi.org/10.1007/s00253-015-6508-2.

Enquist-Newman, M., Faust, A.M.E., Bravo, D.D., Santos, C.N.S., Raisner, R.M., Hanel, A., Sarvabhowman, P., Le, C., Regitsky, D.D., Cooper, S.R., 2014. Efficient ethanol production from brown macroalgae sugars by a synthetic yeast platform. Nature 505, 239–243. https://doi.org/10.1038/nature12771.

Ferdouse, F., Lovestad Holdt, S., Smith, R., Murua, P., Yang, Z., 2018. The global status of seaweed production, trade and utilization. FAO Globefish Research Programme 124, 120. Rome.

Fertah, M., Belfkira, A., Dahmane, E.m., Taourirte, M., Brouillette, F., 2017. Extraction and characterization of sodium alginate from Moroccan *Laminaria digitata* brown seaweed. Arab. J. Chem. 10, S3707–S3714. https://doi.org/10.1016/j.arabjc.2014.05.003.

Follmann, M., Ochrombel, I., Krämer, R., Trötschel, C., Poetsch, A., Rückert, C., Hüser, A., Persicke, M., Seiferling, D., Kalinowski, J., Marin, K., 2009. Functional genomics of pH homeostasis in *Corynebacterium glutamicum* revealed novel links between pH response, oxidative stress, iron homeostasis and methionine synthesis. BMC Genom. 10 https://doi.org/10.1186/1471-2164-10-621, 621-621.

Gießelmann, G., Dietrich, D., Jungmann, L., Kohlstedt, M., Jeon, E.J., Yim, S.S., Sommer, F., Zimmer, D., Mühlhaus, T., Schroda, M., Jeong, K.J., Becker, J., Wittmann, C., 2019. Metabolic engineering of *Corynebacterium glutamicum* for high-level ectoine production: design, combinatorial assembly, and implementation of a transcriptionally balanced heterologous ectoine pathway. Biotechnol. J. 14, 1800417. https://doi.org/10.1002/biot.201800417.

Gläser, L., Kuhl, M., Jovanovic, S., Fritz, M., Vögeli, B., Erb, T.J., Becker, J., Wittmann, C., 2020. A common approach for absolute quantification of short chain CoA thioesters in prokaryotic and eukaryotic microbes. Microb. Cell Factories 19, 160. https://doi.org/10.1186/s12934-020-01413-1.

Goh, C.S., Lee, K.T., 2010. A visionary and conceptual macroalgae-based third-generation bioethanol (TGB) biorefinery in Sabah, Malaysia as an underlay for renewable and sustainable development. Renew. Sustain. Energy Rev. 14, 842–848.

Gopinath, V., Meiswinkel, T.M., Wendisch, V.F., Nampoothiri, K.M., 2011. Amino acid production from rice straw and wheat bran hydrolysates by recombinant pentose-utilizing *Corynebacterium glutamicum*. Appl. Microbiol. Biotechnol. 92, 985–996. https://doi.org/10.1007/s00253-011-3478-x.

Gourdon, P., Baucher, M.F., Lindley, N.D., Guyonvarch, A., 2000. Cloning of the malic enzyme gene from *Corynebacterium glutamicum* and role of the enzyme in lactate metabolism. Appl. Environ. Microbiol. 66, 2981–2987. https://doi.org/10.1128/AEM.66.7.2981-2987.2000.

Guex, N., Diemand, A., Peitsch, M.C., 1999. SWISS-MODEL and the Swiss-Pdb Viewer: an environment for comparative protein modeling. Biochem. Soc. Trans. 18, 2714–2723. https://doi.org/10.1002/elps.1150181505.

Haag, A.L., 2007. Algae bloom again. Nature 447, 520–521. https://doi.org/10.1038/447520a.

Haug, A., Larsen, B., Smidsrød, O., 1974. Uronic acid sequence in alginate from different sources. Carbohydr. Res. 32, 217–225. https://doi.org/10.1016/S0008-6215(00)82100-X.

Hirao, T., Nakano, T., Azuma, T., Sugimoto, M., Nakanishi, T., 1989. L-Lysine production in continuous culture of an L-lysine hyperproducing mutant of *Corynebacterium glutamicum*. Appl. Microbiol. Biotechnol. 32, 269–273. https://doi.org/10.1007/BF00184972.

Hoffmann, S.L., Jungmann, L., Schiefelbein, S., Peyriga, L., Cahoreau, E., Portais, J.-C., Becker, J., Wittmann, C., 2018. Lysine production from the sugar alcohol mannitol: design of the cell factory *Corynebacterium glutamicum* SEA-3 through integrated analysis and engineering of metabolic pathway fluxes. Metab. Eng. 47, 475–487. https://doi.org/10.1016/j.ymben.2018.04.019.

Hou, X., From, N., Angelidaki, I., Huijgen, W.J.J., Bjerre, A.-B., 2017. Butanol fermentation of the brown seaweed *Laminaria digitata* by *Clostridium beijerinckii* DSM-6422. Bioresour. Technol. 238, 16–21. https://doi.org/10.1016/j.biortech.2017.04.035.

Hou, X., Hansen, J.H., Bjerre, A.-B., 2015. Integrated bioethanol and protein production from brown seaweed *Laminaria digitata*. Bioresour. Technol. 197, 310–317. https://doi.org/10.1016/j.biortech.2015.08.091.

HYPERCHEM, 1999. HYPERCHEM version 6.02. 02 Inc, Hypercube, version 6.

Ikeda, M., 2003. Amino acid production processes. Adv. Biochem. Eng. Biotechnol. 79, 1–35. https://doi.org/10.1007/3-540-45989-8_1.

Ikeda, M., 2012. Sugar transport systems in *Corynebacterium glutamicum*: features and applications to strain development. Appl. Microbiol. Biotechnol. 96, 1191–1200. https://doi.org/10.1007/s00253-012-4488-z.

Ikeda, M., 2017. Lysine fermentation: history and genome breeding. In: Yokota, A., Ikeda, M. (Eds.), Amino Acid Fermentation. Springer Japan, Tokyo, pp. 73–102. https://doi.org/10.1007/10_2016_27.

Ikeda, M., Mitsuhashi, S., Tanaka, K., Hayashi, M., 2009. Reengineering of a *Corynebacterium glutamicum* L-arginine and L-citrulline producer. Appl. Environ. Microbiol. 75, 1635–1641. https://doi.org/10.1128/AEM.02027-08.

Jackson, J.B., 2003. Proton translocation by transhydrogenase. FEBS Lett. 545, 18–24. https://doi.org/10.1016/S0014-5793(03)00388-0.

Jäger, W., Schäfer, A., Kalinowski, J., Pühler, A., 1995. Isolation of insertion elements from gram-positive *Brevibacterium, Corynebacterium* and *Rhodococcus* strains using the *Bacillus subtilis sacB* gene as a positive selection marker. FEMS Microbiol. Lett. 126, 1–6. https://doi.org/10.1111/j.1574-6968.1995.tb07381.x.

Jäger, W., Schäfer, A., Pühler, A., Labes, G., Wohlleben, W., 1992. Expression of the *Bacillus subtilis sacB* gene leads to sucrose sensitivity in the gram-positive bacterium *Corynebacterium glutamicum* but not in *Streptomyces lividans*. J. Bacteriol. 174, 5462–5465. https://doi.org/10.1128/jb.174.16.5462-5465.1992.

Kabus, A., Georgi, T., Wendisch, V.F., Bott, M., 2007. Expression of the *Escherichia coli pntAB* genes encoding a membrane-bound transhydrogenase in *Corynebacterium glutamicum* improves L-lysine formation. Appl. Microbiol. Biotechnol. 75, 47–53. https://doi.org/10.1007/s00253-006-0804-9.

Kawai, S., Murata, K., 2016. Biofuel production based on carbohydrates from both brown and red macroalgae: recent developments in key biotechnologies. Int. J. Mol. Sci. 17, 145. https://doi.org/10.3390/ijms17020145.

Kelle, R., Laufer, B., Brunzema, C., Weuster-Botz, D., Krämer, R., Wandrey, C., 1996. Reaction engineering analysis of L-lysine transport by *Corynebacterium glutamicum*. Biotechnol. Bioeng. 51, 40–50. https://doi.org/10.1002/(SICI)1097-0290(19960705)51:1<40::AID-BIT5>3.0.CO;2-0.

Kiefer, P., Heinzle, E., Zelder, O., Wittmann, C., 2004. Comparative metabolic flux analysis of lysine-producing *Corynebacterium glutamicum* cultured on glucose or fructose. Appl. Environ. Microbiol. 70, 229–239. https://doi.org/10.1128/AEM.70.1.229-239.2004.

Kim, N.-J., Li, H., Jung, K., Chang, H.N., Lee, P.C., 2011. Ethanol production from marine algal hydrolysates using *Escherichia coli* KO11. Bioresour. Technol. 102, 7466–7469. https://doi.org/10.1016/j.biortech.2011.04.071.

Kind, S., Jeong, W.K., Schröder, H., Wittmann, C., 2010. Systems-wide metabolic pathway engineering in *Corynebacterium glutamicum* for bio-based production of diaminopentane. Metab. Eng. 12, 341–351. https://doi.org/10.1016/j.ymben.2010.03.005.

Kind, S., Neubauer, S., Becker, J., Yamamoto, M., Völkert, M., von Abendroth, G., Zelder, O., Wittmann, C., 2014. From zero to hero–Production of bio-based nylon from renewable resources using engineered *Corynebacterium glutamicum*. Metab. Eng. 25, 113–123. https://doi.org/10.1016/j.ymben.2014.05.007.

Koffas, M., Stephanopoulos, G., 2005. Strain improvement by metabolic engineering: lysine production as a case study for systems biology. Curr. Opin. Biotechnol. 16, 361–366. https://doi.org/10.1016/j.copbio.2005.04.010.

Kraan, S., 2013. Mass-cultivation of carbohydrate rich macroalgae, a possible solution for sustainable biofuel production. Mitig. Adapt. Strat. Gl. 18, 27–46. https://doi.org/10.1007/s11027-010-9275-5.

Krämer, R., Lambert, C., Hoischen, C., Ebbighausen, H., 1990. Uptake of glutamate in *Corynebacterium glutamicum*. Eur. J. Biochem. 194, 929–935. https://doi.org/10.1111/j.1432-1033.1990.tb19488.x.

Krömer, J.O., Bolten, C.J., Heinzle, E., Schröder, H., Wittmann, C., 2008. Physiological response of *Corynebacterium glutamicum* to oxidative stress induced by deletion of the transcriptional repressor McbR. Microbiol. 154, 3917–3930. https://doi.org/10.1099/mic.0.2008/021204-0.

Lange, A., Becker, J., Schulze, D., Cahoreau, E., Portais, J.-C., Haefner, S., Schröder, H., Krawczyk, J., Zelder, O., Wittmann, C., 2017. Bio-based succinate from sucrose: high-resolution ^{13}C metabolic flux analysis and metabolic engineering of the rumen bacterium *Basfia succiniciproducens*. Metab. Eng. 44, 198–212. https://doi.org/10.1016/j.ymben.2017.10.003.

Laslo, T., von Zaluskowski, P., Gabris, C., Lodd, E., Rückert, C., Dangel, P., Kalinowski, J., Auchter, M., Seibold, G., Eikmanns, B.J., 2012. Arabitol metabolism of *Corynebacterium glutamicum* and its regulation by AtlR. J. Bacteriol. 194, 941–955. https://doi.org/10.1128/JB.06064-11.

Latifi, A.M., Sadegh Nejad, E., Babavalian, H., 2015. Comparison of extraction different methods of sodium alginate from brown alga *Sargassum* sp. localized in the Southern of Iran. J. Appl. Biotechnol. Rep. 2, 251–255.

Lee, S.Y., Park, J., 2010. Integration of systems biology with bioprocess engineering: L-Threonine production by systems metabolic engineering of *Escherichia coli*. Adv. Biochem. Eng. Biotechnol. 120, 1–19. https://doi.org/10.1007/10_2009_57.

Lizée-Prynne, D., López, B., Tala, F., Thiel, M., 2016. No sex-related dispersal limitation in a dioecious, oceanic long-distance traveller: the bull kelp *Durvillaea antarctica*. Bot. Mar. 59, 39–50. https://doi.org/10.1515/bot-2015-0072.

Lynch, M.D., 2016. Into new territory: improved microbial synthesis through engineering of the essential metabolic network. Curr. Opin. Biotechnol. 38, 106–111. https://doi.org/10.1016/j.copbio.2016.01.009.

Manns, D., Nielsen, M.M., Bruhn, A., Saake, B., Meyer, A.S., 2017. Compositional variations of brown seaweeds *Laminaria digitata* and *Saccharina latissima* in Danish waters. J. Appl. Phycol. 29, 1493–1506. https://doi.org/10.1007/s10811-017-1056-z.

Mansilla, A., Ávila, M., Yokoya, N.S., 2012. Current knowledge on biotechnological interesting seaweeds from the Magellan Region, Chile. Rev. Bras. Farmacogn. 22, 760–767. https://doi.org/10.1590/S0102-695X2012005000074.

Mansilla, A.O., Avila, M., Cáceres, J., 2017. Reproductive biology of *Durvillaea antarctica* (chamisso) hariot in the sub-antartic ecoregion of magallanes (51–56° S). J. Appl. Phycol. 29, 2567–2574. https://doi.org/10.1007/s10811-017-1077-7.

Moritz, B., Striegel, K., de Graaf, A.A., Sahm, H., 2000. Kinetic properties of the glucose-6-phosphate and 6 phosphogluconate dehydrogenases from *Corynebacterium glutamicum* and their application for predicting pentose phosphate pathway flux in vivo. Eur. J. Biochem. 267, 3442–3452. https://doi.org/10.1046/j.1432-1327.2000.01354.x.

Naik, S.N., Goud, V.V., Rout, P.K., Dalai, A.K., 2010. Production of first and second generation biofuels: a comprehensive review. Renew. Sustain. Energy Rev. 14, 578–597. https://doi.org/10.1016/j.rser.2009.10.003.

Nielsen, J., 2017. Systems biology of metabolism. Annu. Rev. Biochem. 86, 245–275. https://doi.org/10.1146/annurev-biochem-061516-044757.

Ohnishi, J., Mitsuhashi, S., Hayashi, M., Ando, S., Yokoi, H., Ochiai, K., Ikeda, M., 2002. A novel methodology employing *Corynebacterium glutamicum* genome information to

generate a new L-lysine-producing mutant. Appl. Microbiol. Biotechnol. 58, 217–223. https://doi.org/10.1007/s00253-001-0883-6.

Peng, X., Okai, N., Vertès, A.A., Inatomi, K.-I., Inui, M., Yukawa, H., 2011. Characterization of the mannitol catabolic operon of *Corynebacterium glutamicum*. Appl. Microbiol. Biotechnol. 91, 1375–1387. https://doi.org/10.1007/s00253-011-3352-x.

Poblete-Castro, I., Hoffmann, S., Becker, J., Wittmann, C., 2020. Cascaded valorization of seaweed using microbial cell factories. Curr. Opin. Biotechnol. 65, 102–113. https://doi.org/10.1016/j.copbio.2020.02.008.

Rohles, C.M., Gießelmann, G., Kohlstedt, M., Wittmann, C., Becker, J., 2016. Systems metabolic engineering of *Corynebacterium glutamicum* for the production of the carbon-5 platform chemicals 5-aminovalerate and glutarate. Microb. Cell Factories 15, 154. https://doi.org/10.1186/s12934-016-0553-0.

Rohles, C.M., Gläser, L., Kohlstedt, M., Gießelmann, G., Pearson, S., del Campo, A., Becker, J., Wittmann, C., 2018. A bio-based route to the carbon-5 chemical glutaric acid and to bionylon-6,5 using metabolically engineered *Corynebacterium glutamicum*. Green Chem. 20, 4662–4674. https://doi.org/10.1039/C8GC01901K.

Schiener, P., Black, K.D., Stanley, M.S., Green, D.H., 2015. The seasonal variation in the chemical composition of the kelp species *Laminaria digitata, Laminaria hyperborea, Saccharina latissima* and *Alaria esculenta*. J. Appl. Phycol. 27, 363–373. https://doi.org/10.1007/s10811-014-0327-1.

Schwechheimer, S.K., Becker, J., Peyriga, L., Portais, J.-C., Wittmann, C., 2018. Metabolic flux analysis in *Ashbya gossypii* using ^{13}C-labeled yeast extract: industrial riboflavin production under complex nutrient conditions. Microb. Cell Factories 17, 162. https://doi.org/10.1186/s12934-018-1003-y.

Seibold, G., Auchter, M., Berens, S., Kalinowski, J., Eikmanns, B.J., 2006. Utilization of soluble starch by a recombinant *Corynebacterium glutamicum* strain: growth and lysine production. J. Biotechnol. 124, 381–391. https://doi.org/10.1016/j.jbiotec.2005.12.027.

Sunwoo, I., Kwon, J.E., Jeong, G.-T., Kim, S.-K., 2019. Optimization of hyper-thermal acid hydrolysis and enzymatic saccharification of *Ascophyllum nodosum* for ethanol production with mannitol-adapted yeasts. Bioproc. Biosyst. Eng. 42, 1255–1262. https://doi.org/10.1007/s00449-019-02123-8.

Takeno, S., Hori, K., Ohtani, S., Mimura, A., Mitsuhashi, S., Ikeda, M., 2016. L-Lysine production independent of the oxidative pentose phosphate pathway by *Corynebacterium glutamicum* with the *Streptococcus mutans gapN* gene. Metab. Eng. 37, 1–10. https://doi.org/10.1016/j.ymben.2016.03.007.

Takeno, S., Murata, R., Kobayashi, R., Mitsuhashi, S., Ikeda, M., 2010. Engineering of *Corynebacterium glutamicum* with an NADPH-generating glycolytic pathway for L-lysine production. Appl. Environ. Microbiol. 76, 7154–7160. https://doi.org/10.1128/AEM.01464-10.

Tateno, T., Fukuda, H., Kondo, A., 2007a. Direct production of L-lysine from raw corn starch by *Corynebacterium glutamicum* secreting *Streptococcus bovis* α-amylase using *cspB* promoter and signal sequence. Appl. Microbiol. Biotechnol. 77, 533–541. https://doi.org/10.1007/s00253-007-1191-6.

Tateno, T., Fukuda, H., Kondo, A., 2007b. Production of L-Lysine from starch by *Corynebacterium glutamicum* displaying α-amylase on its cell surface. Appl. Microbiol. Biotechnol. 74, 1213–1220. https://doi.org/10.1007/s00253-006-0766-y.

Torres, M.D., Kraan, S., Domínguez, H., 2019. Seaweed biorefinery. Rev. Environ. Sci. Biotechnol. 18, 335–388. https://doi.org/10.1007/s11157-019-09496-y.

Toyoda, K., Inui, M., 2016. Regulons of global transcription factors in *Corynebacterium glutamicum*. Appl. Microbiol. Biotechnol. 100, 45–60. https://doi.org/10.1007/s00253-015-7074-3.

Uribe, E., Vega-Gálvez, A., Vargas, N., Pasten, A., Rodríguez, K., Ah-Hen, K.S., 2018. Phytochemical components and amino acid profile of brown seaweed *Durvillaea antarctica* as affected by air drying temperature. J. Food Sci. Technol. 55, 4792–4801. https://doi.org/10.1007/s13197-018-3412-7.

van Hal, J.W., Huijgen, W.J.J., López-Contreras, A.M., 2014. Opportunities and challenges for seaweed in the biobased economy. Trends Biotechnol. 32, 231–233. https://doi.org/10.1016/j.tibtech.2014.02.007.

van Winden, W.A., Wittmann, C., Heinzle, E., Heijnen, J.J., 2002. Correcting mass isotopomer distributions for naturally occurring isotopes. Biotechnol. Bioeng. 80, 477–479. https://doi.org/10.1002/bit.10393.

Voegele, R.T., Hahn, M., Lohaus, G., Link, T., Heiser, I., Mendgen, K., 2005. Possible roles for mannitol and mannitol dehydrogenase in the biotrophic plant pathogen *Uromyces fabae*. Plant Physiol. 137, 190, 10.1104 104.051839.

Wargacki, A.J., Leonard, E., Win, M.N., Regitsky, D.D., Santos, C.N.S., Kim, P.B., Cooper, S.R., Raisner, R.M., Herman, A., Sivitz, A.B., Lakshmanaswamy, A., Kashiyama, Y., Baker, D., Yoshikuni, Y., 2012. An engineered microbial platform for direct biofuel production from brown macroalgae. Science 335, 308–313. https://doi.org/10.1126/science.1214547.

Waterhouse, A., Bertoni, M., Bienert, S., Studer, G., Tauriello, G., Gumienny, R., Heer, F. T., de Beer, T.A.P., Rempfer, C., Bordoli, L., Lepore, R., Schwede, T., 2018. SWISS-MODEL: homology modelling of protein structures and complexes. Nucleic Acids Res. 46, W296–W303. https://doi.org/10.1093/nar/gky427.

Wei, N., Quarterman, J., Jin, Y.-S., 2013. Marine macroalgae: an untapped resource for producing fuels and chemicals. Trends Biotechnol. 31, 70–77. https://doi.org/10.1016/j.tibtech.2012.10.009.

Wittmann, C., 2007. Fluxome analysis using GC-MS. Microb. Cell Factories 6. https://doi.org/10.1186/1475-2859-6-6, 6-6.

Wittmann, C., Becker, J., 2007. The L-Lysine Story: from metabolic pathways to industrial production. In: Wendisch, V. (Ed.), Amino Acid Biosynthesis - Pathways, Regulation and Metabolic Engineering, vol. 5. Springer Berlin Heidelberg, pp. 39–70. https://doi.org/10.1007/7171_2006_089.

Wittmann, C., Hans, M., Heinzle, E., 2002. In vivo analysis of intracellular amino acid labelings by GC/MS. Anal. Biochem. 307, 379–382. https://doi.org/10.1016/S0003-2697(02)00030-1.

Wittmann, C., Hans, M., van Winden, W.A., Ras, C., Heijnen, J.J., 2005. Dynamics of intracellular metabolites of glycolysis and TCA cycle during cell-cycle-related oscillation in *Saccharomyces cerevisiae*. Biotechnol. Bioeng. 89, 839–847. https://doi.org/10.1002/bit.20408.

Wittmann, C., Kiefer, P., Zelder, O., 2004. Metabolic fluxes in *Corynebacterium glutamicum* during lysine production with sucrose as carbon source. Appl. Environ. Microbiol. 70, 7277–7287. https://doi.org/10.1128/AEM.70.12.7277-7287.2004.

Xu, J.-Z., Ruan, H.-Z., Yu, H.-B., Liu, L.-M., Zhang, W., 2020. Metabolic engineering of carbohydrate metabolism systems in *Corynebacterium glutamicum* for improving the efficiency of L-lysine production from mixed sugar. Microb. Cell Factories 19, 39. https://doi.org/10.1186/s12934-020-1294-7.

Xu, J.-Z., Wu, Z.-H., Gao, S.-J., Zhang, W., 2018. Rational modification of tricarboxylic acid cycle for improving L-lysine production in *Corynebacterium glutamicum*. Microb. Cell Factories 17, 105. https://doi.org/10.1186/s12934-018-0958-z.

Xu, J., Zhang, J., Guo, Y., Zai, Y., Zhang, W., 2013. Improvement of cell growth and L-lysine production by genetically modified *Corynebacterium glutamicum* during growth on molasses. J. Ind. Microbiol. Biotechnol. 40, 1423–1432. https://doi.org/10.1007/s10295-013-1329-8.

Yamauchi, Y., Hirasawa, T., Nishii, M., Furusawa, C., Shimizu, H., 2014. Enhanced acetic acid and succinic acid production under microaerobic conditions by *Corynebacterium glutamicum* harboring *Escherichia coli* transhydrogenase gene *pntAB*. J. Gen. Appl. Microbiol. 60, 112–118. https://doi.org/10.2323/jgam.60.112.

Yokota, A., Lindley, N.D., 2005. Central metabolism: sugar uptake and conversion. In: Eggeling, L., Bott, M. (Eds.), Handbook of *Corynebacterium Glutamicum*. CRC Press, Boca Raton, pp. 215–240.

Zhan, M., Kan, B., Dong, J., Xu, G., Han, R., Ni, Y., 2019. Metabolic engineering of *Corynebacterium glutamicum* for improved L-arginine synthesis by enhancing NADPH supply. J. Ind. Microbiol. Biotechnol. 46, 45–54. https://doi.org/10.1007/s10295-018-2103-8.

Zhang, X., Yao, L., Xu, G., Zhu, J., Zhang, X., Shi, J., Xu, Z., 2017. Enhancement of fructose utilization from sucrose in the cell for improved L-serine production in engineered *Corynebacterium glutamicum*. Biochem. Eng. J. 118, 113–122. https://doi.org/10.1016/j.bej.2016.11.021.